

Thermochemical Non-Equilibrium Reentry Flows in Two-Dimensions: Eleven Species Model – Part I

EDISSON SÁVIO DE GÓES MACIEL⁽¹⁾ and AMILCAR PORTO PIMENTA⁽²⁾

IEA – Aeronautical Engineering Division

ITA – Aeronautical Technological Institute

Praça Mal. do Ar Eduardo Gomes, 50 – Vila das Acácias – São José dos Campos – SP – 12228-900
BRAZIL

⁽¹⁾edisavio@edissonsavio.eng.br ⁽¹⁾<http://www.edissonsavio.eng.br> and ⁽²⁾amilcar@ita.br

Abstract: - This work describes the thermochemical non-equilibrium simulations of reactive flow in two-dimensions. The Van Leer and Liou and Steffen Jr. schemes, in their first- and second-order versions, are implemented to accomplish the numerical simulations. The Euler and Navier-Stokes equations, on a finite volume context and employing structured and unstructured spatial discretizations, are applied to solve the “hot gas” hypersonic flows around a blunt body, around a double ellipse, and around a reentry capsule in two-dimensions. The second-order version of the Van Leer and Liou and Steffen Jr. schemes are obtained from a “MUSCL” extrapolation procedure in a context of structured spatial discretization. In the unstructured context, only first-order solutions are presented. The convergence process is accelerated to the steady state condition through a spatially variable time step procedure, which has proved effective gains in terms of computational acceleration (Maciel). The reactive simulations involve a Earth atmosphere chemical model of eleven species: N, O, N₂, O₂, NO, N⁺, O⁺, N₂⁺, O₂⁺, NO⁺ and e⁻, based on the works of Dunn and Kang and of Park. Thirty-two, to the former, and fourth-three, to the latter, chemical reactions, involving dissociation, recombination and ionization, are simulated by the proposed models. The Arrhenius formula is employed to determine the reaction rates and the law of mass action is used to determine the source terms of each gas species equation. The results have indicated the Van Leer scheme as the most accurate one, both inviscid and viscous cases.

Key-Words: - Thermochemical non-equilibrium, Earth reentry, Eleven species model, Hypersonic “hot gas” flow, Finite volume, Euler and Navier-Stokes equations, Two-dimensions.

1 Introduction

A hypersonic flight vehicle has many applications for both military and civilian purposes including reentry vehicles such as the Space Shuttle and the Automated Transfer Vehicle (ATV) of the European Space Agency (ESA). The extreme environment of a hypersonic flow has a major impact on the design and analysis of the aerodynamic and thermal loading of a reentry or hypersonic cruise vehicle. During a hypersonic flight, the species of the flow field are vibrationally excited, dissociated, and ionized because of the very strong shock wave which is created around a vehicle. Because of these phenomena, it is necessary to consider the flow to be in thermal and chemical non-equilibrium.

In high speed flows, any adjustment of chemical composition or thermodynamic equilibrium to a change in local environment requires certain time. This is because the redistribution of chemical species and internal energies require certain number of molecular collisions, and hence a certain characteristic time. Chemical non-equilibrium occurs when the characteristic time for the chemical reactions to reach local equilibrium is of the same

order as the characteristic time of the fluid flow. Similarly, thermal non-equilibrium occurs when the characteristic time for translation and various internal energy modes to reach local equilibrium is of the same order as the characteristic time of the fluid flow. Since chemical and thermal changes are the results of collisions between the constituent particles, non-equilibrium effects prevail in high-speed flows in low-density air.

In chemical non-equilibrium flows the mass conservation equation is applied to each of the constituent species in the gas mixture. Therefore, the overall mass conservation equation is replaced by as many species conservation equations as the number of chemical species considered. The assumption of thermal non-equilibrium introduces additional energy conservation equations – one for every additional energy mode. Thus, the number of governing equations for non-equilibrium flow is much bigger compared to those for perfect gas flow. A complete set of governing equations for non-equilibrium flow may be found in [1-2].

Analysis of non-equilibrium flow is rather complex because (1) the number of equations to be

solved is much larger than the Navier-Stokes equations, and (2) there are additional terms like the species production, mass diffusion, and vibrational energy relaxation, etc., that appear in the governing equations. In a typical flight of the NASP (National AeroSpace Plane) flying at Mach 15, ionization is not expected to occur, and a 5-species air is adequate for the analysis (see [3]). Since the rotational characteristic temperatures for the constituent species (namely N, O, N₂, O₂ and NO) are small, the translational and rotational energy modes are assumed to be in equilibrium, whereas the vibrational energy mode is assumed to be in non-equilibrium. [4] has simplified the thermodynamic model by assuming a harmonic oscillator to describe the vibrational energy. Ionic species and electrons are not considered. This simplifies the set of governing equations by eliminating the equation governing electron and electronic excitation energy. [4] has taken the complete set of governing equations from [1], and simplified them for a five-species two-temperature air model.

The problems of chemical non-equilibrium in the shock layers over vehicles flying at high speeds and high altitudes in the Earth's atmosphere have been discussed by several investigators ([5-8]). Most of the existing computer codes for calculating the non-equilibrium reacting flow use the one-temperature model, which assumes that all of the internal energy modes of the gaseous species are in equilibrium with the translational mode ([7-8]). It has been pointed out that such a one-temperature description of the flow leads to a substantial overestimation of the rate of equilibrium because of the elevated vibrational temperature [6]. A three-temperature chemical-kinetic model has been proposed by [9] to describe the relaxation phenomena correctly in such a flight regime. However, the model is quite complex and requires many chemical rate parameters which are not yet known. As a compromise between the three-temperature and the conventional one-temperature model, a two-temperature chemical-kinetic model has been developed ([10-11]), which is designated herein as the TT_v model. The TT_v model uses one temperature T to characterize both the translational energy of the atoms and molecules and the rotational energy of the molecules, and another temperature T_v to characterize the vibrational energy of the molecules, translational energy of the electrons, and electronic excitation energy of atoms and molecules. The model has been applied to compute the thermodynamic properties behind a normal shock wave in a flow through a constant-area duct ([10-

11]). Radiation emission from the non-equilibrium flow has been calculated using the Non-equilibrium Air Radiation (NEQAIR) program ([12-13]). The flow and the radiation computations have been packaged into a single computer program, the Shock-Tube Radiation Program (STRAP) ([11]).

A first-step assessment of the TT_v model was made in [11] where it was used in computing the flow properties and radiation emission from the flow in a shock tube for pure nitrogen undergoing dissociation and weak ionization (ionization fraction less than 0.1%). Generally good agreement was found between the calculated radiation emission and those obtained experimentally in shock tubes ([14-16]). The only exception involved the vibrational temperature. The theoretical treatment of the vibrational temperature could not be validated because the existing data on the vibrational temperature behind a normal shock wave ([16]) are those for an electronically excited state of the molecular nitrogen ion N₂⁺ instead of the ground electronic state of the neutral nitrogen molecule N₂ which is calculated in the theoretical model. The measured vibrational temperature of N₂⁺ was much smaller than the calculated vibrational temperature for N₂.

In 2012, [17-18] started to research the high temperature gas effects in the Earth atmosphere. They have presented a numerical tool implemented to simulate inviscid and viscous flows employing the reactive gas formulation of thermal and chemical non-equilibrium. The Euler and Navier-Stokes equations, employing a finite volume formulation, on the context of structured and unstructured spatial discretizations, were solved. These variants have allowed an effective comparison between the two types of spatial discretization aiming verify their potentialities: solution quality, convergence speed, computational cost, etc. The aerospace problem involving the hypersonic flow around a blunt body, in two-dimensions, was simulated. The reactive simulations have involved an air chemical model of five species: N, O, N₂, O₂ and NO. Seventeen chemical reactions, involving dissociation and recombination, were simulated by the proposed model, suggested by [19]. The Arrhenius formula was employed to determine the reaction rates and the law of mass action was used to obtain the source terms of each gas species equation. Good results were obtained.

In 2012 yet, [20-21] have presented a numerical tool implemented to simulate inviscid and viscous flows employing the reactive gas formulation of thermochemical non-equilibrium using a seven

species chemical model. The Euler and Navier-Stokes equations, employing a finite volume formulation, on the context of structured and unstructured spatial discretizations, were solved. The aerospace problem involving the hypersonic flow around a blunt body, in two-dimensions, was simulated. The reactive simulations have involved an air chemical model of seven species: N, O, N₂, O₂, NO, NO⁺ and e⁻. Eighteen chemical reactions, involving dissociation, recombination and ionization, were simulated by the proposed model. This model was suggested by [22]. The Arrhenius formula was employed to determine the reaction rates and the law of mass action was used to determine the source terms of each gas species equation. Good results were obtained.

This work, first of this study, describes a numerical tool to perform thermochemical non-equilibrium simulations of reactive flow in two-dimensions, using an eleven species chemical model. The [23-24] schemes, in their first- and second-order versions, are implemented to accomplish the numerical simulations. The Euler and Navier-Stokes equations, on a finite volume context and employing structured and unstructured spatial discretizations, are applied to solve the “hot gas” hypersonic flows around a blunt body, around a double ellipse, and around a reentry capsule in two-dimensions. The second-order versions of the [23-24] schemes are obtained from a “MUSCL” extrapolation procedure in a context of structured spatial discretization. In terms of unstructured spatial discretization, only first-order solutions are presented. The convergence process is accelerated to the steady state condition through a spatially variable time step procedure, which has proved effective gains in terms of computational acceleration (see [25-26]). In this paper, the structured and unstructured formulations are shown, whereas the results are presented in part two.

The reactive simulations involve an air chemical model of eleven species: N, O, N₂, O₂, NO, N⁺, O⁺, N₂⁺, O₂⁺, NO⁺ and e⁻. Thirty-two (32) or Fourth-three (43) chemical reactions, involving dissociation, recombination and ionization, are simulated by the proposed models of [27-28], respectively. The Arrhenius formula is employed to determine the reaction rates and the law of mass action is used to determine the source terms of each gas species equation.

2 Navier-Stokes Equations

The reactive Navier-Stokes equations in thermal and chemical non-equilibrium can be implemented on a

finite volume context, in the two-dimensional space. In this case, these equations in integral and conservative forms can be expressed by:

$$\frac{\partial}{\partial t} \int_V Q dV + \int_S \vec{F} \cdot \vec{n} dS = \int_V S_{CV} dV, \text{ with} \\ \vec{F} = (E_e - E_v) \vec{i} + (F_e - F_v) \vec{j}, \quad (1)$$

where: Q is the vector of conserved variables, V is the volume of a computational cell, \vec{F} is the complete flux vector, \vec{n} is the unity vector normal to the flux face, S is the flux area, S_{CV} is the chemical and vibrational source term, E_e and F_e are the convective flux vectors or the Euler flux vectors in the x and y directions, respectively, E_v and F_v are the viscous flux vectors in the x and y directions, respectively. The \vec{i} and \vec{j} unity vectors define the Cartesian coordinate system. Fifteen (15) conservation equations are solved: one of general mass conservation, two of linear momentum conservation, one of total energy, ten of species mass conservation and one of the vibrational internal energy of the molecules. Therefore, one of the species is absent of the iterative process. To the present study, in which is chosen a chemical model to the air composed of eleven (11) chemical species (N, O, N₂, O₂, NO, N⁺, O⁺, N₂⁺, O₂⁺, NO⁺ and e⁻), thirty-two (32) chemical reactions, due to the [27] model, or fourth-three (43) chemical reactions, due to the [28] model, this species can be either the N₂ or the O₂. To this work, it was chosen the N₂. The vectors Q, E_e, F_e, E_v, F_v and S_{CV} can, hence, be defined as follows ([4]):

$$Q = \begin{Bmatrix} \rho \\ \rho u \\ \rho v \\ e \\ \rho_1 \\ \rho_2 \\ \rho_4 \\ \rho_5 \\ \rho_6 \\ \rho_7 \\ \rho_8 \\ \rho_9 \\ \rho_{10} \\ \rho_{11} \\ \rho e_v \end{Bmatrix}, \quad E_e = \begin{Bmatrix} \rho u \\ \rho u^2 + p \\ \rho uv \\ \rho Hu \\ \rho_1 u \\ \rho_2 u \\ \rho_4 u \\ \rho_5 u \\ \rho_6 u \\ \rho_7 u \\ \rho_8 u \\ \rho_9 u \\ \rho_{10} u \\ \rho_{11} u \\ \rho e_{v,u} \end{Bmatrix}, \quad F_e = \begin{Bmatrix} \rho v \\ \rho uv \\ \rho v^2 + p \\ \rho Hv \\ \rho_1 v \\ \rho_2 v \\ \rho_4 v \\ \rho_5 v \\ \rho_6 v \\ \rho_7 v \\ \rho_8 v \\ \rho_9 v \\ \rho_{10} v \\ \rho_{11} v \\ \rho e_{v,v} \end{Bmatrix}; \quad (2)$$

$$E_v = \frac{1}{Re} \left\{ \begin{array}{c} 0 \\ \tau_{xx} \\ \tau_{xy} \\ \tau_{xx}u + \tau_{xy}v - q_{f,x} - q_{v,x} - \phi_x \\ -\rho_1 V_{1x} \\ -\rho_2 V_{2x} \\ -\rho_4 V_{4x} \\ -\rho_5 V_{5x} \\ -\rho_6 V_{6x} \\ -\rho_7 V_{7x} \\ -\rho_8 V_{8x} \\ -\rho_9 V_{9x} \\ -\rho_{10} V_{10x} \\ -\rho_{11} V_{11x} \\ -q_{v,x} - \phi_{v,x} \end{array} \right\}; \quad (3)$$

$$F_v = \frac{1}{Re} \left\{ \begin{array}{c} 0 \\ \tau_{xy} \\ \tau_{yy} \\ \tau_{xy}u + \tau_{yy}v - q_{f,y} - q_{v,y} - \phi_y \\ -\rho_1 V_{1y} \\ -\rho_2 V_{2y} \\ -\rho_4 V_{4y} \\ -\rho_5 V_{5y} \\ -\rho_6 V_{6y} \\ -\rho_7 V_{7y} \\ -\rho_8 V_{8y} \\ -\rho_9 V_{9y} \\ -\rho_{10} V_{10y} \\ -\rho_{11} V_{11y} \\ -q_{v,y} - \phi_{v,y} \end{array} \right\}; \quad (4)$$

in which: ρ is the mixture density; u and v are Cartesian components of the velocity vector in the x and y directions, respectively; p is the fluid static pressure; e is the fluid total energy; $\rho_1, \rho_2, \rho_4, \rho_5, \rho_6, \rho_7, \rho_8, \rho_9, \rho_{10}, \rho_{11}$ are densities of the $N, O, O_2, NO, N^+, O^+, N_2^+, O_2^+, NO^+$ and e^- , respectively; H is the mixture total enthalpy; e_v is the sum of the vibrational energy of the molecules; the τ 's are the components of the viscous stress tensor; $q_{f,x}$ and $q_{f,y}$ are the frozen components of the Fourier-heat-flux vector in the x and y directions, respectively; $q_{v,x}$ and $q_{v,y}$ are the components of the Fourier-heat-flux vector calculated with the vibrational thermal conductivity and vibrational temperature; $\rho_s v_{sx}$ and $\rho_s v_{sy}$ represent the species diffusion flux, defined by the Fick law;

$$S_{CV} = \left\{ \begin{array}{c} 0 \\ 0 \\ 0 \\ 0 \\ \dot{\omega}_1 \\ \dot{\omega}_2 \\ \dot{\omega}_4 \\ \dot{\omega}_5 \\ \dot{\omega}_6 \\ \dot{\omega}_7 \\ \dot{\omega}_8 \\ \dot{\omega}_9 \\ \dot{\omega}_{10} \\ \dot{\omega}_{11} \\ \sum_{s=mol} \rho_s (e_{v,s}^* - e_{v,s}) / \tau_s + \sum_{s=mol} \dot{\omega}_s e_{v,s} \end{array} \right\} \quad (5)$$

ϕ_x and ϕ_y are the terms of mixture diffusion; $\phi_{v,x}$ and $\phi_{v,y}$ are the terms of molecular diffusion calculated at the vibrational temperature; $\dot{\omega}_s$ is the chemical source term of each species equation, defined by the law of mass action; e_v^* is the molecular-vibrational-internal energy calculated with the translational/rotational temperature; and τ_s is the translational-vibrational characteristic relaxation time of each molecule.

The frozen components of the Fourier-heat-flux vector, which considers only thermal conduction, are defined by:

$$q_{f,x} = -k_{f,TR} \frac{\partial T}{\partial x} \quad \text{and} \quad q_{f,y} = -k_{f,TR} \frac{\partial T}{\partial y}, \quad (6)$$

where $k_{f,TR}$ is the mixture frozen translational / rotational thermal conductivity, calculated conform presented in section 4.4. The vibrational components of the Fourier-heat-flux vector are calculated as follows:

$$q_{v,x} = -k_{f,VE} \frac{\partial T_v}{\partial x} \quad \text{and} \quad q_{v,y} = -k_{f,VE} \frac{\partial T_v}{\partial y}, \quad (7)$$

in which $k_{f,VE}$ is the mixture frozen vibrational/electronic thermal conductivity and T_v is the vibrational temperature, what characterizes this model as of two temperatures: translational / rotational and vibrational. The calculation of $k_{f,VE}$ is also presented in section 4.4.

The terms of species diffusion, defined by the Fick law, to a condition of thermal non-equilibrium, are determined by ([4]):

$$\rho_s v_{sx} = -\rho D_s \frac{\partial Y_{MF,s}}{\partial x} \quad \text{and} \quad \rho_s v_{sy} = -\rho D_s \frac{\partial Y_{MF,s}}{\partial y}, \quad (8)$$

with “s” referent to a given species, $Y_{MF,s}$ being the molar fraction of the species, defined as:

$$Y_{MF,s} = \frac{\rho_s / M_s}{\sum_{k=1}^{ns} \rho_k / M_k} \quad (9)$$

and D_s is the species-effective-diffusion coefficient.

The diffusion terms ϕ_x and ϕ_y which appear in the energy equation are defined by ([19]):

$$\phi_x = \sum_{s=1}^{ns} \rho_s v_{sx} h_s \quad \text{and} \quad \phi_y = \sum_{s=1}^{ns} \rho_s v_{sy} h_s, \quad (10)$$

being h_s the specific enthalpy (sensible) of the chemical species “s”. The molecular diffusion terms calculated at the vibrational temperature, $\phi_{v,x}$ and $\phi_{v,y}$, which appear in the vibrational-internal-energy equation are defined by ([4]):

$$\phi_{v,x} = \sum_{s=mol} \rho_s v_{sx} h_{v,s} \quad \text{and} \quad \phi_{v,y} = \sum_{s=mol} \rho_s v_{sy} h_{v,s}, \quad (11)$$

with $h_{v,s}$ being the specific enthalpy (sensible) of the chemical species “s” calculated at the vibrational temperature T_v . The sum of Eq. (11), as also those present in Eq. (5), considers only the molecules of the system, namely: N_2 , O_2 , NO , N_2^+ , O_2^+ , and NO^+ .

3 Thermodynamics Properties

3.1. Definition of general parameters

$$p = RT \sum_{s=1}^{ns} \rho_s / M_s = \rho \sigma RT \therefore \rho \sigma = \sum_{s=1}^{ns} \rho_s / M_s = \rho \sum_{s=1}^{ns} c_s / M_s \Rightarrow \sigma = \sum_{s=1}^{ns} c_s / M_s, \quad (12)$$

in which: σ is the mixture number in kg-mol/kg and c_s is the mass fraction (non-dimensional), defined by $c_s = \rho_s / \rho$.

$$\sigma = \sum_{s=1}^{ns} \sigma_s \Rightarrow \sigma_s = c_s / M_s;$$

$$M_{mixt} = 1/\sigma \therefore M_{mixt} = 1 / \sum_{s=1}^{ns} c_s / M_s; \quad (13a)$$

$$e_{v,s}^* = e_{v,s}(T_v = T), \quad (13b)$$

with: σ_s being the number of kg-mol/kg of species “s” and M_{mixt} is the mixture molecular mass, in kg/kg-mol.

3.2. Thermodynamic model

(a) Mixture translational internal energy:

$$e_T = \sum_{s=1}^{ns} e_{T,s} \sigma_s = \sum_{s=1}^{ns} \left[\int_0^T C_{v,T,s}(T') dT' + h^0 \right] \sigma_s, \quad (14)$$

where: $e_{T,s}$ is the translational internal energy per kg-mol of species “s”, in J/kg-mol. The specific heat at constant volume per kg-mol of species “s” due to translation, in J/(kg-mol.K), is defined by:

$$C_{v,T,s}(T) = 1.5R. \quad (15)$$

Hence,

$$e_{T,s}(T) = 1.5RT + h^0 \Rightarrow e_T(T) = \sum_{s=1}^{ns} \sigma_s (1.5RT + h^0), \quad (16)$$

with: e_T being the translational internal energy per unity of the gaseous mixture mass, in J/kg, and h^0 being the formation enthalpy of the species “s” per kg-mol of species, J/kg-mol. It is important to note that:

$$e_T(T) = \sum_{s=1}^{ns} \sigma_s (1.5RT + h^0) = \sum_{s=1}^{ns} c_s \left(1.5 \frac{R}{M_s} T + \frac{h^0}{M_s} \right) = \sum_{s=1}^{ns} c_s (1.5R_s T + h_s^0) \Rightarrow e_T(T) = \sum_{s=1}^{ns} c_s (1.5R_s T + h_s^0), \quad (17)$$

with: R_s being the gas constant of species “s” and h_s^0 being the formation enthalpy of species “s” in J/kg. The species formation enthalpy per g-mol of species is specified in Tab. 1. As can be noted, dividing each above term by the species molecular mass and multiplying by 10^3 , it is possible to obtain the formation enthalpy in J/kg. The species molecular weights in g/g-mol are obtained from [3] and are presented in Tab. 2.

Table 1. Species formation enthalpy.

Species	h^0 (J/g-mol)
N	472,586.98
O	249,132.10
N ₂	0.0
O ₂	0.0
NO	90,378.17
N ⁺	1,881,582.46
O ⁺	1,568,443.53
N ₂ ⁺	1,526,905.61
O ₂ ⁺	1,172,398.22
NO ⁺	992,963.20
e ⁻	0.0

Table 2. Molecular weight of the chemical species.

Species	Molecular Weight (g/g-mol)
N	14.0
O	16.0
N ₂	28.0
O ₂	32.0
NO	30.0
N ⁺	14.0
O ⁺	16.0
N ₂ ⁺	28.0
O ₂ ⁺	32.0
NO ⁺	30.0
e ⁻	0.0005486

(b) Mixture rotational internal energy:

$$e_R = \sum_{s=1}^{ns} e_{R,s} \sigma_s = \sum_{s=1}^{ns} \left[\int_0^T C_{v,R,s}(T') dT' \right] \sigma_s = \sum_{s=1}^{ns} \sigma_s \int_0^T C_{v,R,s}(T') dT', \quad (18)$$

where: $e_{R,s}$ is the rotational internal energy per kg-mol of species “s”, in J/kg-mol. The specific heat at constant volume per kg-mol of species “s” due to rotation, in J/(kg-mol.K), is defined by:

$$C_{v,R,s} = R \Rightarrow e_{R,s}(T) = RT \therefore e_R(T) = \sum_{s=1}^{ns} \sigma_s RT$$

or $e_R(T) = \sum_{s=1}^{ns} c_s R_s T, \quad (19)$

with e_R being the rotational internal energy per unity of gaseous mixture mass, in J/kg.

(c) Mixture vibrational internal energy:

$$e_V = \sum_{s=1}^{ns} e_{v,s} \sigma_s = \sum_{s=1}^{ns} \sigma_s \int_0^{T_V} C_{v,V,s}(T') dT'; \quad \text{with}$$

$$C_{v,V,s} = C_{v,V,s}(T_V) = R \frac{e^{\theta_{v,s}/T_V}}{(e^{\theta_{v,s}/T_V} - 1)^2} \left(\frac{\theta_{v,s}}{T_V} \right)^2, \quad (20)$$

in which: e_V is the vibrational internal energy per unity of gaseous mixture mass, in J/kg; $e_{v,s}$ is the vibrational internal energy per kg-mol of species “s”, in J/kg-mol; $C_{v,V,s}$ is the specific heat at constant volume per kg-mol of species “s” due to vibration, in J/(kg-mol.K); $\theta_{v,s}$ is the characteristic vibrational temperature of species “s”, in K; and T_V is the vibrational temperature, in K. The characteristic vibrational temperature to each molecule is specified in Tab. 3, obtained from [28]. It is important to note that e_V is also directly obtained from the vector of conserved variables.

Table 3. Characteristic vibrational temperature of the molecular species.

Species	$\theta_{v,s}$ (K)
N ₂	3,390.0
O ₂	2,270.0
NO	2,740.0
N ₂ ⁺	3,390.0
O ₂ ⁺	2,270.0
NO ⁺	2,740.0

It is important to note that the modes of translational and rotational internal energy are assumed completely excited and, hence, the specific heats at constant volume to these modes are temperature independent. The vibrational-internal-energy mode is admitted not be completely excited, and, hence, the vibrational specific heat at constant volume is function of the vibrational temperature. The expression above to $C_{v,V,s}$ is due to [29] and is the result of the hypothesis that the molecules can be considered as harmonic oscillators. Note that when the mode of vibrational internal energy is completely excited, i.e., when $T_V \gg \theta_{v,s}$, $C_{v,V,s} = R$.

(d) Species characteristic electronic temperatures and degeneracies:

The complete eleven species model uses an approximation to consider electronic contribution. The degeneracies of the microstates that form the

most probable macrostate are considered, together with the characteristic electronic temperatures associated with.

Table 4 presents the degeneracies and the characteristic electronic temperatures. This is a form to consider electronic contribution in the present two-temperature formulation; or better, one considers two-temperature formulation as composed of translational / rotational contribution and vibrational / electronic contribution. In despite of not considering a third temperature, electronic temperature, one considers the traditional two-temperature model and, in the transport properties calculation, evaluates the electronic contribution. Moreover, in the calculation of the vibrational temperature the consideration of the electronic mode is also taken into account, allowing a better approximation of the electronic state. In the determination of the boundary conditions, the total energy is calculated based on the sums of the vibrational and electronic energies. These procedures try to simulate the electronic contributions, as emphasized above.

Table 4. Degeneracies and characteristic electronic temperature of the species.

Species	Level	g	$\bar{\theta}_{s,i}$ (K)
N	0	4	0.0
	1	10	$2.766469645581980 \times 10^4$
	2	6	$4.149309313560210 \times 10^4$
O	0	5	0.0
	1	3	$2.277077570280000 \times 10^2$
	2	1	$3.265688785704000 \times 10^2$
	3	5	$2.283028632262240 \times 10^4$
	4	1	$4.861993036434160 \times 10^4$
N ₂	0	0	0.0
	1	1	0.0
	2	3	$7.223156514095200 \times 10^4$
	3	6	$8.577862640384000 \times 10^4$
	4	6	$8.605026716160000 \times 10^4$
	5	3	$9.535118627874400 \times 10^4$
	6	1	$9.805635702203200 \times 10^4$
	7	2	$9.968267656935200 \times 10^4$
	8	2	$1.048976467715200 \times 10^5$
	9	5	$1.116489555200000 \times 10^5$
	10	1	$1.225836470400000 \times 10^5$
	11	6	$1.248856873600000 \times 10^5$
	12	6	$1.282476158188320 \times 10^5$
	13	10	$1.338060936000000 \times 10^5$
	14	6	$1.404296391107200 \times 10^5$
15	6	$1.504958859200000 \times 10^5$	

Table 4. Degeneracies and characteristic electronic temperature of the species. (Continuation)

Species	Level	g	$\bar{\theta}_{s,i}$ (K)
O ₂	0	3	0.0
	1	2	$1.139156019700800 \times 10^4$
	2	1	$1.898473947826400 \times 10^4$
	3	1	$4.755973576639200 \times 10^4$
	4	6	$4.991242097343200 \times 10^4$
	5	3	$5.092268575561600 \times 10^4$
	6	3	$7.189863255967200 \times 10^4$
NO	0	4	0.0
	1	8	$5.467345760000000 \times 10^4$
	2	2	$6.317139627802400 \times 10^4$
	3	4	$6.599450342445600 \times 10^4$
	4	4	$6.906120960000000 \times 10^4$
	5	4	$7.049998480000000 \times 10^4$
	6	4	$7.491055017560000 \times 10^4$
	7	2	$7.628875293968000 \times 10^4$
	8	4	$8.676188537552000 \times 10^4$
	9	2	$8.714431182368000 \times 10^4$
	10	4	$8.886077063728000 \times 10^4$
	11	4	$8.981755614528000 \times 10^4$
	12	2	$8.988445919208000 \times 10^4$
	13	2	$9.042702132000000 \times 10^4$
	14	2	$9.064283760000000 \times 10^4$
	15	4	$9.111763341600000 \times 10^4$
N ⁺	0	1	0.0
	1	3	$7.006835224000000 \times 10^1$
	2	5	$1.881917961600000 \times 10^2$
	3	5	$2.203656871824000 \times 10^4$
	4	1	$4.703183475776000 \times 10^4$
	5	5	$6.731252222192000 \times 10^4$
	6	15	$1.327190797527310 \times 10^5$
O ⁺	0	4	0.0
	1	10	$3.858334678336000 \times 10^4$
	2	6	$5.822349152848000 \times 10^4$
N ₂ ⁺	0	2	0.0
	1	4	$1.318997164600000 \times 10^4$
	2	2	$3.663323087728000 \times 10^4$
	3	4	$3.668876760000000 \times 10^4$
	4	8	$5.985304832000000 \times 10^4$
	5	8	$6.618365920000000 \times 10^4$
	6	4	$7.598991933064000 \times 10^4$
	7	4	$7.625508560000000 \times 10^4$
	8	4	$8.201018640000000 \times 10^4$
	9	4	$8.416834920000000 \times 10^4$
	10	8	$8.632651200000000 \times 10^4$
	11	8	$8.920406240000000 \times 10^4$
	12	4	$9.208161280000000 \times 10^4$
	13	4	$9.222549032000000 \times 10^4$
	14	2	$9.293768404400000 \times 10^4$
	15	2	$9.639793840000000 \times 10^4$
	16	4	$1.035918144000000 \times 10^5$

Table 4. Degeneracies and characteristic electronic temperature of the species.
(Continuation)

Species	Level	g	$\bar{\theta}_{s,i}$ (K)
O_2^+	0	4	0.0
	1	8	$4.735440815760000 \times 10^4$
	2	4	$5.837398741440000 \times 10^4$
	3	6	$5.841427312000000 \times 10^4$
	4	4	$6.229896616000000 \times 10^4$
	5	2	$6.733467936000000 \times 10^4$
	6	4	$7.121937240000000 \times 10^4$
	7	4	$7.654284064000000 \times 10^4$
	8	4	$8.819691976000000 \times 10^4$
	9	4	$8.891630736000000 \times 10^4$
	10	8	$9.423977560000000 \times 10^4$
	11	4	$9.495916320000000 \times 10^4$
	12	2	$9.592026503360000 \times 10^4$
	13	2	$9.985099888000000 \times 10^4$
14	4	$1.035918144000000 \times 10^5$	
NO^+	0	1	0.0
	1	3	$7.508967768000000 \times 10^4$
	2	6	$8.525462447640000 \times 10^4$
	3	6	$8.903572570160000 \times 10^4$
	4	3	$9.746982592400000 \times 10^4$
	5	1	$1.000553049584000 \times 10^5$
	6	2	$1.028033655904000 \times 10^5$
	7	2	$1.057138639424800 \times 10^5$

(e) Mixture internal energy:

$$e_{\text{int}} = e_T + e_R + e_V, \quad (21)$$

which is the internal energy per unity of mixture mass, in J/kg.

(f) Frozen speed of sound:

$$C_{v,TR} = \sum_{s=1}^{ns} \sigma_s C_{v,TR,s} = \sum_{s=1}^{ns} \sigma_s \begin{pmatrix} 2.5R & \text{molecules} \\ 1.5R & \text{atoms and } e^- \end{pmatrix};$$

$$\beta = R\sigma/C_{v,TR} \quad \therefore a_f = \sqrt{(\beta+1)p/\rho}. \quad (22)$$

The frozen speed of sound, in a thermochemical non-equilibrium model, should be employed in the calculation of the convective flux of the [23-24] schemes. $C_{v,TR,s}$ is the specific heat at constant volume due to translation and rotation; in other words, $C_{v,TR,s}$ is the sum of $C_{v,T,s}$ with $C_{v,R,s}$.

(g) Determination of the translational/rotational temperature:

$$\frac{e}{\rho} = \sum_{s=1}^{ns} c_s C_{v,TR,s} T + \sum_{s=1}^{ns} c_s h_s^0 + e_v + e_{el} + \frac{1}{2}(u^2 + v^2), \quad (23)$$

to the two-dimensional case. Hence, noting that T is constant at the right hand side of Eq. (23), it is possible to write:

$$T = \frac{1}{\sum_{s=1}^{ns} c_s C_{v,TR,s}} \left[\frac{e}{\rho} - \sum_{s=1}^{ns} c_s h_s^0 - e_v - e_{el} - \frac{1}{2}(u^2 + v^2) \right], \quad (24)$$

to the two-dimensional case;

(h) Determination of the vibrational temperature:

The vibrational temperature is calculated through an interactive process employing the Newton-Raphson method.

(i) Species pressure:

Applying the equation of a thermally perfect gas to each species:

$$p_s = \rho_s R_s T, \quad (25)$$

where: $\rho_s = c_s \rho$ is the density of species "s", R_s is the gas constant to species "s" and T is the translational/rotational temperature.

4 Transport Properties

4.1. Collision integrals to species i and j

In Table 5 are presented values of $\text{Log}_{10}[\pi\Omega_{i,j}^{(1,1)}]$ and $\text{Log}_{10}[\pi\Omega_{i,j}^{(2,2)}]$ to temperature values of 2,000 K and 4,000 K. The indexes i and j indicate, in the present case, the collision partners; in other words, the pair formed by one atom and one atom, one atom and one molecule, etc. These data were obtained from [3].

The data aforementioned define a linear interpolation to values of $\text{Log}_{10}[\pi\Omega_{i,j}^{(k,k)}]$ as function of $\text{Ln}(T)$, with $k = 1, 2$, through the linear equation:

$$\text{Log}_{10}[\pi\Omega_{i,j}^{(k,k)}](T) = \text{Log}_{10}[\pi\Omega_{i,j}^{(k,k)}](T = 2,000\text{K}) + \text{slope} \times \text{Ln}(T/2,000), \quad (26)$$

in which:

$$\text{slope} = \left\{ \text{Log}_{10} [\pi\Omega_{i,j}^{(k,k)}] (T = 4,000\text{K}) - \text{Log}_{10} [\pi\Omega_{i,j}^{(k,k)}] (T = 2,000\text{K}) \right\} / \text{Ln}2. \quad (27)$$

with the value of $\Omega_{i,j}^{(k,k)}$ in m^2 .

Table 5. Collision integrals to eleven chemical species: N, O, N₂, O₂, NO, N⁺, O⁺, N₂⁺, O₂⁺, NO⁺ and e⁻.

Pairs		Log ₁₀ [πΩ _{i,j} ^(1,1)]		Log ₁₀ [πΩ _{i,j} ^(2,2)]	
i	j	2,000 K	4,000 K	2,000 K	4,000 K
N	N	-14.08	-14.11	-14.74	-14.82
N	O	-14.76	-14.86	-14.69	-14.80
N	N ₂	-14.67	-14.75	-14.59	-14.66
N	O ₂	-14.66	-14.74	-14.59	-14.66
N	NO	-14.66	-14.75	-14.67	-14.66
N	N ⁺	-14.08	-14.11	-14.37	-14.49
N	O ⁺	-14.34	-14.46	-14.38	-14.50
N	N ₂ ⁺	-14.34	-12.19	-14.38	-14.50
N	O ₂ ⁺	-14.34	-12.19	-14.38	-14.50
N	NO ⁺	-14.34	-14.46	-14.38	-14.50
N	e ⁻	-15.30	-15.30	-15.30	-15.30
O	N	-14.76	-14.86	-14.69	-14.80
O	O	-14.11	-14.14	-14.71	-14.79
O	N ₂	-14.63	-14.72	-14.55	-14.64
O	O ₂	-14.69	-14.76	-14.62	-14.69
O	NO	-14.66	-14.74	-14.59	-14.66
O	N ⁺	-14.34	-14.46	-14.38	-14.50
O	O ⁺	-14.11	-14.14	-14.50	-14.58
O	N ₂ ⁺	-14.34	-14.46	-14.38	-14.50
O	O ₂ ⁺	-14.34	-14.46	-14.38	-14.50
O	NO ⁺	-14.34	-14.46	-14.38	-14.50
O	e ⁻	-15.94	-15.82	-15.94	-15.82
N ₂	N	-14.67	-14.75	-14.59	-14.66
N ₂	O	-14.63	-14.72	-14.55	-14.64
N ₂	N ₂	-14.56	-14.65	-14.50	-14.58
N ₂	O ₂	-14.58	-14.63	-14.51	-14.54
N ₂	NO	-14.57	-14.64	-14.51	-14.56
N ₂	N ⁺	-14.34	-14.46	-14.38	-14.50
N ₂	O ⁺	-14.34	-14.46	-14.38	-14.50
N ₂	N ₂ ⁺	-14.34	-14.46	-14.38	-14.50
N ₂	O ₂ ⁺	-14.34	-14.46	-14.38	-14.50
N ₂	NO ⁺	-14.34	-14.46	-14.38	-14.50
N ₂	e ⁻	-15.11	-15.02	-15.11	-15.02

Table 5. Collision integrals to eleven chemical species: N, O, N₂, O₂, NO, N⁺, O⁺, N₂⁺, O₂⁺, NO⁺ and e⁻. (Continuation)

Pairs		Log ₁₀ [πΩ _{i,j} ^(1,1)]		Log ₁₀ [πΩ _{i,j} ^(2,2)]	
i	j	2,000 K	4,000 K	2,000 K	4,000 K
O ₂	N	-14.66	-14.74	-14.59	-14.66
O ₂	O	-14.69	-14.76	-14.62	-14.69
O ₂	N ₂	-14.58	-14.63	-14.51	-14.54
O ₂	O ₂	-14.60	-14.64	-14.54	-14.57
O ₂	NO	-14.59	-14.63	-14.52	-14.56
O ₂	N ⁺	-14.34	-14.46	-14.38	-14.50
O ₂	O ⁺	-14.34	-14.46	-14.38	-14.50
O ₂	N ₂ ⁺	-14.34	-14.46	-14.38	-14.50
O ₂	O ₂ ⁺	-14.34	-14.46	-14.38	-14.50
O ₂	NO ⁺	-14.34	-14.46	-14.38	-14.50
O ₂	e ⁻	-15.52	-15.39	-15.52	-15.39
NO	N	-14.66	-14.75	-14.67	-14.66
NO	O	-14.66	-14.74	-14.59	-14.66
NO	N ₂	-14.57	-14.64	-14.51	-14.56
NO	O ₂	-14.59	-14.63	-14.52	-14.56
NO	NO	-14.58	-14.64	-14.52	-14.56
NO	N ⁺	-14.34	-14.46	-14.38	-14.50
NO	O ⁺	-14.34	-14.46	-14.38	-14.50
NO	N ₂ ⁺	-14.34	-14.46	-14.38	-14.50
NO	O ₂ ⁺	-14.34	-14.46	-14.38	-14.50
NO	NO ⁺	-14.18	-14.22	-14.38	-14.50
NO	e ⁻	-15.30	-15.08	-15.30	-15.08
N ⁺	N	-14.08	-14.11	-14.37	-14.49
N ⁺	O	-14.34	-14.46	-14.38	-14.50
N ⁺	N ₂	-14.34	-14.46	-14.38	-14.50
N ⁺	O ₂	-14.34	-14.46	-14.38	-14.50
N ⁺	NO	-14.34	-14.46	-14.38	-14.50
N ⁺	N ⁺	-11.70	-12.19	-11.49	-11.98
N ⁺	O ⁺	-11.70	-12.19	-11.49	-11.98
N ⁺	N ₂ ⁺	-11.70	-12.19	-11.49	-11.98
N ⁺	O ₂ ⁺	-11.70	-12.19	-11.49	-11.98
N ⁺	NO ⁺	-11.70	-12.19	-11.49	-11.98
N ⁺	e ⁻	-11.70	-12.19	-11.49	-11.98

The value of $\pi\Omega_{i,j}^{(k,k)}$ is obtained from:

$$\pi\Omega_{i,j}^{(k,k)}(T) = e^{\left\{ \text{Log}_{10} [\pi\Omega_{i,j}^{(k,k)}] (T=2,000\text{K}) + \text{slope} \times \text{Ln}(T/2,000) \right\} \times \text{Ln}10}, \quad (28)$$

Table 5. Collision integrals to eleven chemical species: N, O, N₂, O₂, NO, N⁺, O⁺, N₂⁺, O₂⁺, NO⁺ and e⁻. (Continuation)

Pairs		Log ₁₀ [πΩ _{i,j} ^(1,1)]		Log ₁₀ [πΩ _{i,j} ^(2,2)]	
i	j	2,000 K	4,000 K	2,000 K	4,000 K
O ⁺	N	-14.34	-14.46	-14.38	-14.50
O ⁺	O	-14.11	-14.14	-14.45	-14.58
O ⁺	N ₂	-14.34	-14.46	-14.38	-14.50
O ⁺	O ₂	-14.34	-14.46	-14.38	-14.50
O ⁺	NO	-14.34	-14.46	-14.38	-14.50
O ⁺	N ⁺	-11.70	-12.19	-11.49	-11.98
O ⁺	O ⁺	-11.70	-12.19	-11.49	-11.98
O ⁺	N ₂ ⁺	-11.70	-12.19	-11.49	-11.98
O ⁺	O ₂ ⁺	-11.70	-12.19	-11.49	-11.98
O ⁺	NO ⁺	-11.70	-12.19	-11.49	-11.98
O ⁺	e ⁻	-11.70	-12.19	-11.49	-11.98
N ₂ ⁺	N	-14.34	-12.19	-14.38	-14.50
N ₂ ⁺	O	-14.34	-14.46	-14.38	-14.50
N ₂ ⁺	N ₂	-14.34	-14.46	-14.38	-14.50
N ₂ ⁺	O ₂	-14.34	-14.46	-14.38	-14.50
N ₂ ⁺	NO	-14.34	-14.46	-14.38	-14.50
N ₂ ⁺	N ⁺	-11.70	-12.19	-11.49	-11.98
N ₂ ⁺	O ⁺	-11.70	-12.19	-11.49	-11.98
N ₂ ⁺	N ₂ ⁺	-11.70	-12.19	-11.49	-11.98
N ₂ ⁺	O ₂ ⁺	-11.70	-12.19	-11.49	-11.98
N ₂ ⁺	NO ⁺	-11.70	-12.19	-11.49	-11.98
N ₂ ⁺	e ⁻	-11.70	-12.19	-11.49	-11.98
O ₂ ⁺	N	-14.34	-12.19	-14.38	-14.50
O ₂ ⁺	O	-14.34	-14.46	-14.38	-14.50
O ₂ ⁺	N ₂	-14.34	-14.46	-14.38	-14.50
O ₂ ⁺	O ₂	-14.34	-14.46	-14.38	-14.50
O ₂ ⁺	NO	-14.34	-14.46	-14.38	-14.50
O ₂ ⁺	N ⁺	-11.70	-12.19	-11.49	-11.98
O ₂ ⁺	O ⁺	-11.70	-12.19	-11.49	-11.98
O ₂ ⁺	N ₂ ⁺	-11.70	-12.19	-11.49	-11.98
O ₂ ⁺	O ₂ ⁺	-11.70	-12.19	-11.49	-11.98
O ₂ ⁺	NO ⁺	-11.70	-12.19	-11.49	-11.98
O ₂ ⁺	e ⁻	-11.70	-12.19	-11.49	-11.98

Table 5. Collision integrals to eleven chemical species: N, O, N₂, O₂, NO, N⁺, O⁺, N₂⁺, O₂⁺, NO⁺ and e⁻. (Continuation)

Pairs		Log ₁₀ [πΩ _{i,j} ^(1,1)]		Log ₁₀ [πΩ _{i,j} ^(2,2)]	
i	j	2,000 K	4,000 K	2,000 K	4,000 K
NO ⁺	N	-14.34	-14.46	-14.38	-14.50
NO ⁺	O	-14.34	-14.46	-14.38	-14.50
NO ⁺	N ₂	-14.34	-14.46	-14.38	-14.50
NO ⁺	O ₂	-14.34	-14.46	-14.38	-14.50
NO ⁺	NO	-14.18	-14.22	-14.38	-14.50
NO ⁺	N ⁺	-11.70	-12.19	-11.49	-11.98
NO ⁺	O ⁺	-11.70	-12.19	-11.49	-11.98
NO ⁺	N ₂ ⁺	-11.70	-12.19	-11.49	-11.98
NO ⁺	O ₂ ⁺	-11.70	-12.19	-11.49	-11.98
NO ⁺	NO ⁺	-11.70	-12.19	-11.49	-11.98
NO ⁺	e ⁻	-11.70	-12.19	-11.49	-11.98
e ⁻	N	-15.30	-15.30	-15.30	-15.30
e ⁻	O	-15.94	-15.82	-15.94	-15.82
e ⁻	N ₂	-15.11	-15.02	-15.11	-15.02
e ⁻	O ₂	-15.52	-15.39	-15.52	-15.39
e ⁻	NO	-15.30	-15.08	-15.30	-15.08
e ⁻	N ⁺	-11.70	-12.19	-11.49	-11.98
e ⁻	O ⁺	-11.70	-12.19	-11.49	-11.98
e ⁻	N ₂ ⁺	-11.70	-12.19	-11.49	-11.98
e ⁻	O ₂ ⁺	-11.70	-12.19	-11.49	-11.98
e ⁻	NO ⁺	-11.70	-12.19	-11.49	-11.98
e ⁻	e ⁻	-11.70	-12.19	-11.49	-11.98

4.2. Modified collision integrals to the species i and j

[3-4] define the modified collision integrals to the species i and j as:

$$\Delta_{i,j}^{(1)}(T) = \frac{8}{3} \sqrt{\frac{2m_{i,j}}{\pi RT}} \pi \Omega_{i,j}^{(1,1)} \quad \text{and} \quad \Delta_{i,j}^{(2)}(T) = \frac{16}{5} \sqrt{\frac{2m_{i,j}}{\pi RT}} \pi \Omega_{i,j}^{(2,2)}, \quad (29)$$

with:

$$m_{i,j} = M_i M_j / (M_i + M_j), \quad (30)$$

being the reduced molecular mass. These integrals are given in m.s. With the definition of the modified collision integrals to species i and j, it is possible to define the mixture transport properties (viscosity and thermal conductivities) and the species diffusion property (diffusion coefficient).

4.3. Mixture molecular viscosity

[4] defines the mixture molecular viscosity as:

$$\mu_{\text{mixt}} = \sum_{i=1}^{ns} \frac{m_i \sigma_i}{\sum_{j=1}^{ns} \sigma_j \Delta_{i,j}^{(2)}(T)}, \quad (31)$$

where:

$$m_i = M_i / N_{AV}, \quad (32)$$

being the mass of a species particle under study;

$N_{AV} = 6.022045 \times 10^{23}$ particles/g-mol, Avogadro number. This mixture molecular viscosity is given in kg/(m.s).

4.4. Translational, rotational, vibrational / electronic, and electron thermal conductivities

All thermal conductivities are expressed in J/(m.s.K). [4] defines the mixture vibrational, rotational and translational thermal conductivities, as also the species diffusion coefficient, as follows.

(a) Translational thermal conductivity:

The mode of translational internal energy is admitted completely excited; hence, the thermal conductivity of the translational internal energy is determined by:

$$k_T = \frac{15}{4} k_{\text{Boltzmann}} \sum_{i=1}^{ns-1} \frac{\sigma_i}{\sum_{j=1}^{ns-1} \bar{a}_{i,j} \sigma_j \Delta_{i,j}^{(2)}(T) + 3.54 \times \bar{a}_{i,e} \sigma_e \Delta_{i,e}^{(2)}(T_v)}, \quad (33)$$

in which:

$k_{\text{Boltzmann}} = 1,380622 \times 10^{-23} \text{J/K} = \text{Boltzmann constant}$;

$$\bar{a}_{i,j} = 1 + \frac{(1 - M_i/M_j)[0.45 - 2.54(M_i/M_j)]}{(1 + M_i/M_j)^2}. \quad (34)$$

In this work is also implemented an alternate translational thermal conductivity, which generates a second version of the eleven species model. This second version is referred in this text as the “incomplete” model. The second option is defined as:

$$k_T = \frac{15}{4} k_{\text{Boltzmann}} \sum_{i=1}^{ns} \frac{\sigma_i}{\sum_{j=1}^{ns} \bar{a}_{i,j} \sigma_j \Delta_{i,j}^{(2)}(T)}. \quad (35)$$

(b) Rotational thermal conductivity:

The mode of rotational internal energy is also considered fully excited; hence, the thermal conductivity due to rotational internal energy is defined by:

$$k_R = k_{\text{Boltzmann}} \sum_{i=\text{mol}} \frac{\sigma_i}{\sum_{j=1}^{ns-1} \sigma_j \Delta_{i,j}^{(1)}(T) + \sigma_e \Delta_{i,e}^{(1)}(T_v)}. \quad (36)$$

(c) Frozen translational / rotational thermal conductivity:

$$k_{f,TR} = k_T + k_R. \quad (37)$$

(d) Thermal conductivity due to molecular vibration and electronic excitation:

The mode of vibrational internal energy, however, is assumed be partially excited. The vibrational / electronic thermal conductivity is calculated according to [1]. Firstly, one has to calculate the contribution of each molecule to the conductivity:

$$S = \sum_{i=\text{mol}} \frac{\sigma_i}{\sum_{j=1}^{ns-1} \sigma_j \Delta_{i,j}^{(1)}(T) + \sigma_e \Delta_{i,e}^{(1)}(T_v)}. \quad (38)$$

To considerate the specific heat at constant volume for the electronic contribution, it is necessary to take into account the number of degeneracies of each atom and molecule, as well the electronic temperatures that each degeneracy is associated with. The complete specific heat at constant volume is defined as:

$$C_{v,VE} = \sum_{s=1}^{ns} c_s (C_{v,V,s}/R + C_{v,E,s}), \quad (39)$$

with $C_{v,V,s}$ obtained from Eq. (20). The $C_{v,E,s}$ is obtained by:

$$C_{v,E,s} = \sum_{i=1}^{nd} g_{s,i} \left(\frac{\bar{\theta}_{s,i}}{T_v} \right)^2 e^{-\bar{\theta}_{s,i}/T_v} / \sum_{i=0}^{nd} g_{s,i} e^{-\bar{\theta}_{s,i}/T_v} - \quad (40a)$$

$$\sum_{i=1}^{nd} g_{s,i} \bar{\theta}_{s,i} e^{-\bar{\theta}_{s,i}/T_v} \times \sum_{i=0}^{nd} g_{s,i} \left(\frac{\bar{\theta}_{s,i}}{T_v} \right) e^{-\bar{\theta}_{s,i}/T_v} \left/ \left(\sum_{i=0}^{nd} g_{s,i} e^{-\bar{\theta}_{s,i}/T_v} \right)^2 \right., \quad (40b)$$

where: “s” is the species under consideration and “nd” is the number of degeneracies of each microstate. The vibrational / electronic thermal conductivity is determined by:

$$k_{VE} = k_{\text{Boltzmann}} \times C_{v,VE} \times S. \quad (41)$$

To the incomplete model, one has:

$$k_v = k_{\text{Boltzmann}} \sum_{i=\text{mol}}^{ns-1} \frac{(C_{v,v,i}/R)\sigma_i}{\sum_{j=1}^{ns} \sigma_j \Delta_{i,j}^{(1)}(T) + \sigma_e \Delta_{i,e}^{(1)}(T_v)}, \quad (42)$$

(e) Thermal conductivity due to electron:

The electron conductivity is considered in the complete model and is given by

$$k_e = \frac{15}{4} k_{\text{Boltzmann}} \frac{\sigma_e}{\sum_{j=1}^{ns} \sigma_j \Delta_{e,j}^{(2)}(T_v)}. \quad (43)$$

(f) Frozen vibrational / electronic thermal conductivity:

$$k_{f,VE} = k_{VE} + k_e. \quad (44)$$

To the incomplete model,

$$k_{f,VE} = k_v. \quad (44)$$

4.5 Species diffusion coefficient

The mass-diffusion-effective coefficient, D_i , of the species “i” in the gaseous mixture is defined by:

$$D_i = \frac{\sigma^2 M_i (1 - \sigma_i M_i)}{\sum_{\substack{j=1 \\ j \neq i}}^{ns-1} \sigma_j / D_{i,j} + \sigma_e / D_{i,e}}, \quad (45)$$

$$D_{i,j} = \frac{k_{\text{Boltzmann}} T}{p \Delta_{i,j}^{(1)}(T)} \quad \text{and} \quad D_{i,e} = \frac{k_{\text{Boltzmann}} T_v}{p \Delta_{i,e}^{(1)}(T_v)}, \quad (46)$$

where: $D_{i,j}$ is the binary diffusion coefficient to a pair of particles of the species “i” and “j” and is related with the modified collision integral conform

described above, in Eq. (46). This coefficient is measured in m^2/s .

To the incomplete model, one has:

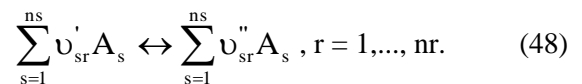
$$D_i = \frac{\sigma^2 M_i (1 - \sigma_i M_i)}{\sum_{j=1}^{ns} \sigma_j / D_{i,j}}. \quad (47)$$

5 Chemical Model

The chemical models employed to this case of thermochemical non-equilibrium are the eleven species models of [27-28], using the N, O, N₂, O₂, NO, N⁺, O⁺, N₂⁺, O₂⁺, NO⁺ and e⁻ species. These formulations use, in the calculation of the species production rates, a temperature of reaction rate control, introduced in the place of the translational / rotational temperature. This procedure aims a couple between vibration and dissociation. This temperature is defined as: $T_{\text{rc}} = \sqrt{T \times T_v}$, where T is the translational / rotational temperature and T_v is the vibrational temperature. This temperature T_{rc} replaces the translational / rotational temperature in the calculation of the species production rates, according to [28].

5.1. Law of Mass Action

The symbolic representation of a given reaction in the present work follows the [30] formulation and is represented by:



The law of mass action applied to this system of chemical reactions is defined by:

$$\dot{\omega}_s = M_s \sum_{r=1}^{nr} (\nu_{sr}'' - \nu_{sr}') \left\{ k_{fr} \prod_{s=1}^{ns} \left(\frac{\rho_s}{M_s} \right)^{\nu_{sr}'} - k_{br} \prod_{s=1}^{ns} \left(\frac{\rho_s}{M_s} \right)^{\nu_{sr}''} \right\}, \quad (49)$$

where A_s represents the chemical symbol of species “s”, “ns” is the number of species of the present study (reactants and products) involved in the considered reaction; “nr” is the number of reactions considered in the chemical model; ν_{sr}' e ν_{sr}'' are the stoichiometric coefficients to reactants and products, respectively; $k_{fr} = AT^B e^{-C/T}$ and $k_{br} = DT^{-E}$, with A, B, C, D and E being constants of a specific

chemical reaction under study [“fr” = forward reaction and “br” = backward reaction]. It is important to note that $k_{br} = k_{fr}/k_{er}$, with k_{er} being the equilibrium constant which depends only of the thermodynamic quantities.

(a) Dunn and Kang’s model:

The first chemical model is due to [27]. The chemical reactions involve dissociation, recombination, exchange and ionization.

Table 6. Chemical reactions and forward coefficients.

Reaction	Forward reaction rate coefficients, k_{fr} , $\text{cm}^3/(\text{mol.s})$	Third body
$\text{O}_2 + \text{M} \leftrightarrow 2\text{O} + \text{M}$	$3.60 \times 10^{18} T^{-1.0} e^{(-59,500/T)}$	N, NO
$\text{O}_2 + \text{O} \leftrightarrow 3\text{O}$	$9.00 \times 10^{19} T^{-1.0} e^{(-59,500/T)}$	-
$2\text{O}_2 \leftrightarrow 2\text{O} + \text{O}_2$	$3.24 \times 10^{19} T^{-1.0} e^{(-59,500/T)}$	-
$\text{O}_2 + \text{N}_2 \leftrightarrow 2\text{O} + \text{N}_2$	$7.20 \times 10^{18} T^{-1.0} e^{(-59,500/T)}$	-
$\text{N}_2 + \text{M} \leftrightarrow 2\text{N} + \text{M}$	$1.90 \times 10^{17} T^{0.5} e^{(-113,000/T)}$	O, NO, O_2
$\text{N}_2 + \text{N} \leftrightarrow 2\text{N} + \text{N}$	$4.085 \times 10^{22} T^{-1.5} e^{(-113,000/T)}$	-
$2\text{N}_2 \leftrightarrow 2\text{N} + \text{N}_2$	$4.70 \times 10^{17} T^{0.5} e^{(-113,000/T)}$	-
$\text{NO} + \text{M} \leftrightarrow \text{N} + \text{O} + \text{M}$	$3.90 \times 10^{20} T^{-1.5} e^{(-75,500/T)}$	O_2 , N_2
$\text{NO} + \text{M} \leftrightarrow \text{N} + \text{O} + \text{M}$	$7.80 \times 10^{21} T^{-1.5} e^{(-75,500/T)}$	N, O, NO
$\text{NO} + \text{O} \leftrightarrow \text{O}_2 + \text{N}$	$3.20 \times 10^9 T^{1.0} e^{(-19,700/T)}$	-
$\text{N}_2 + \text{O} \leftrightarrow \text{NO} + \text{N}$	$7.00 \times 10^{13} e^{(-38,000/T)}$	-
$\text{O}_2^+ + \text{O} \leftrightarrow \text{O}_2 + \text{O}^+$	$2.92 \times 10^{18} T^{1.11} e^{(-28,000/T)}$	-
$\text{N}_2 + \text{N}^+ \leftrightarrow \text{N}_2^+ + \text{N}$	$2.02 \times 10^{11} T^{0.81} e^{(-13,000/T)}$	-
$\text{NO}^+ + \text{O} \leftrightarrow \text{NO} + \text{O}^+$	$3.63 \times 10^{15} T^{-0.6} e^{(-50,800/T)}$	-
$\text{N}_2 + \text{O}^+ \leftrightarrow \text{N}_2^+ + \text{O}$	$3.40 \times 10^{19} T^{-2.0} e^{(-23,000/T)}$	-
$\text{NO}^+ + \text{O}_2 \leftrightarrow \text{NO} + \text{O}_2^+$	$1.80 \times 10^{15} T^{-0.17} e^{(-33,000/T)}$	-
$\text{NO}^+ + \text{N} \leftrightarrow \text{NO} + \text{N}^+$	$1.00 \times 10^{19} T^{-0.93} e^{(-61,000/T)}$	-
$\text{N} + \text{O} \leftrightarrow \text{NO}^+ + e^-$	$1.40 \times 10^6 T^{1.5} e^{(-31,900/T)}$	-
$2\text{O} \leftrightarrow \text{O}_2^+ + e^-$	$1.60 \times 10^{17} T^{-0.98} e^{(-80,800/T)}$	-
$2\text{N} \leftrightarrow \text{N}_2^+ + e^-$	$1.40 \times 10^{13} e^{(-67,800/T)}$	-
$\text{O} + e^- \leftrightarrow \text{O}^+ + 2e^-$	$3.60 \times 10^{31} T^{-2.91} e^{(-158,000/T)}$	-
$\text{N} + e^- \leftrightarrow \text{N}^+ + 2e^-$	$1.10 \times 10^{32} T^{-3.14} e^{(-169,000/T)}$	-
$\text{O}_2 + \text{N}_2 \leftrightarrow \text{NO} + \text{NO}^+ + e^-$	$1.38 \times 10^{20} T^{-1.84} e^{(-141,000/T)}$	-
$\text{N}_2 + \text{NO} \leftrightarrow \text{N}_2 + \text{NO}^+ + e^-$	$2.20 \times 10^{15} T^{-0.35} e^{(-108,000/T)}$	-
$\text{NO}^+ + \text{O} \leftrightarrow \text{O}_2 + \text{N}^+$	$1.34 \times 10^{13} T^{-0.31} e^{(-77,270/T)}$	-
$\text{O}_2 + \text{NO} \leftrightarrow \text{NO}^+ + \text{O}_2 + e^-$	$8.80 \times 10^{16} T^{-0.35} e^{(-108,000/T)}$	-

Table 7. Chemical reactions and backward coefficients.

Reaction	Backward reaction rate coefficients, k_{br} , $\text{cm}^3/(\text{mol.s})$ or $\text{cm}^6/(\text{mol}^2.\text{s})$	Third body
$\text{O}_2 + \text{M} \leftrightarrow 2\text{O} + \text{M}$	$3.00 \times 10^{15} T^{-0.5}$	N, NO
$\text{O}_2 + \text{O} \leftrightarrow 3\text{O}$	$7.50 \times 10^{16} T^{-0.5}$	-
$2\text{O}_2 \leftrightarrow 2\text{O} + \text{O}_2$	$2.70 \times 10^{16} T^{-0.5}$	-
$\text{O}_2 + \text{N}_2 \leftrightarrow 2\text{O} + \text{N}_2$	$6.00 \times 10^{15} T^{-0.5}$	-
$\text{N}_2 + \text{M} \leftrightarrow 2\text{N} + \text{M}$	$1.10 \times 10^{16} T^{-0.5}$	O, NO, O_2
$\text{N}_2 + \text{N} \leftrightarrow 2\text{N} + \text{N}$	$2.27 \times 10^{21} T^{-1.5}$	-
$2\text{N}_2 \leftrightarrow 2\text{N} + \text{N}_2$	$2.72 \times 10^{16} T^{-0.5}$	-
$\text{NO} + \text{M} \leftrightarrow \text{N} + \text{O} + \text{M}$	$1.00 \times 10^{20} T^{-1.5}$	O_2 , N_2
$\text{NO} + \text{M} \leftrightarrow \text{N} + \text{O} + \text{M}$	$2.00 \times 10^{21} T^{-1.5}$	N, O, NO
$\text{NO} + \text{O} \leftrightarrow \text{O}_2 + \text{N}$	$1.30 \times 10^{10} T^{-1.0} e^{(-3,580/T)}$	-
$\text{N}_2 + \text{O} \leftrightarrow \text{NO} + \text{N}$	1.56×10^{13}	-
$\text{O}_2^+ + \text{O} \leftrightarrow \text{O}_2 + \text{O}^+$	$7.80 \times 10^{11} T^{0.5}$	-
$\text{N}_2 + \text{N}^+ \leftrightarrow \text{N}_2^+ + \text{N}$	$7.80 \times 10^{11} T^{0.5}$	-
$\text{NO}^+ + \text{O} \leftrightarrow \text{NO} + \text{O}^+$	1.50×10^{13}	-
$\text{N}_2 + \text{O}^+ \leftrightarrow \text{N}_2^+ + \text{O}$	$2.48 \times 10^{19} T^{-2.2}$	-
$\text{NO}^+ + \text{O}_2 \leftrightarrow \text{NO} + \text{O}_2^+$	$1.80 \times 10^{13} T^{-0.5}$	-
$\text{NO}^+ + \text{N} \leftrightarrow \text{NO} + \text{N}^+$	4.80×10^{14}	-
$\text{N} + \text{O} \leftrightarrow \text{NO}^+ + e^-$	$6.70 \times 10^{21} T^{-1.5}$	-
$2\text{O} \leftrightarrow \text{O}_2^+ + e^-$	$8.00 \times 10^{21} T^{-1.5}$	-
$2\text{N} \leftrightarrow \text{N}_2^+ + e^-$	$1.50 \times 10^{22} T^{-1.5}$	-
$\text{O} + e^- \leftrightarrow \text{O}^+ + 2e^-$	$2.20 \times 10^{40} T^{-4.5}$	-
$\text{N} + e^- \leftrightarrow \text{N}^+ + 2e^-$	$2.20 \times 10^{40} T^{-4.5}$	-
$\text{O}_2 + \text{N}_2 \leftrightarrow \text{NO} + \text{NO}^+ + e^-$	$1.00 \times 10^{24} T^{-2.5}$	-
$\text{N}_2 + \text{NO} \leftrightarrow \text{N}_2 + \text{NO}^+ + e^-$	$2.20 \times 10^{26} T^{-2.5}$	-
$\text{NO}^+ + \text{O} \leftrightarrow \text{O}_2 + \text{N}^+$	1.00×10^{14}	-
$\text{O}_2 + \text{NO} \leftrightarrow \text{NO}^+ + \text{O}_2 + e^-$	$8.80 \times 10^{26} T^{-2.5}$	-

In this model, thirty-two chemical reactions are simulated. These reactions involve dissociation, recombination, exchange and ionization. It corresponds to $n_s = 11$ and $n_r = 32$. Table 6 presents the values to A, B, C, D and E for the forward reaction rates of the 32 chemical reactions. Table 7 presents the values to A, B, C, D and E for the backward reaction rates.

(b) Park’s model:

The second chemical model is due to [28]. The chemical reactions also involve dissociation, recombination, exchange and ionization. [28] model calculate the backward coefficients considering the

equilibrium constant concept. The equilibrium constant is calculated by:

$$k_e = e^{(B_1+B_2 \ln(Z)+B_3Z+B_4Z^2+B_5Z^3)} \quad (50)$$

where:

$$Z = 10,000/T.$$

The backward reaction rate coefficient is determined by the following equation:

$$k_b = k_f/k_e. \quad (51)$$

Table 8. Chemical reactions and forward coefficients.

Reaction	Forward reaction rate coefficients, k_{fr} , $\text{cm}^3/(\text{mol.s})$	Third body
$\text{O}_2+\text{M}\leftrightarrow 2\text{O}+\text{M}$	$2.90 \times 10^{23} T^{-2.0} e^{(-59,750/T)}$	N, O
$\text{O}_2+\text{M}\leftrightarrow 2\text{O}+\text{M}$	$9.68 \times 10^{22} T^{-2.0} e^{(-59,750/T)}$	$\text{N}_2, \text{O}_2, \text{NO}, \text{N}^+, \text{O}^+, \text{N}_2^+, \text{O}_2^+, \text{NO}^+$
$\text{N}_2+\text{N}\leftrightarrow 2\text{N}+\text{N}$	$1.60 \times 10^{22} T^{-1.6} e^{(-113,200/T)}$	-
$\text{N}_2+\text{O}\leftrightarrow 2\text{N}+\text{O}$	$4.98 \times 10^{22} T^{-1.6} e^{(-113,200/T)}$	-
$\text{N}_2+\text{M}\leftrightarrow 2\text{N}+\text{M}$	$3.70 \times 10^{21} T^{-1.6} e^{(-113,200/T)}$	N_2, O_2
$\text{N}_2+\text{NO}\leftrightarrow 2\text{N}+\text{NO}$	$4.98 \times 10^{21} T^{-1.6} e^{(-113,200/T)}$	-
$\text{N}_2+\text{M}\leftrightarrow 2\text{N}+\text{M}$	$8.30 \times 10^{24} T^{-1.6} e^{(-113,200/T)}$	$\text{N}^+, \text{O}^+, \text{N}_2^+, \text{O}_2^+, \text{NO}^+$
$\text{NO}+\text{M}\leftrightarrow \text{N}+\text{O}+\text{M}$	$7.95 \times 10^{23} T^{-2.0} e^{(-75,500/T)}$	$\text{N}, \text{O}, \text{N}_2, \text{O}_2, \text{NO}, \text{N}^+, \text{O}^+, \text{N}_2^+, \text{O}_2^+, \text{NO}^+$
$\text{NO}+\text{O}\leftrightarrow \text{O}_2+\text{N}$	$8.37 \times 10^{12} e^{(-19,450/T)}$	-
$\text{N}_2+\text{O}\leftrightarrow \text{NO}+\text{N}$	$6.44 \times 10^{17} T^{-1.0} e^{(-38,370/T)}$	-
$\text{O}_2^++\text{O}\leftrightarrow \text{O}_2+\text{O}^+$	$6.85 \times 10^{15} T^{-0.52} e^{(-18,600/T)}$	-
$\text{N}_2+\text{N}^+\leftrightarrow \text{N}_2^++\text{N}$	$9.85 \times 10^{12} T^{-0.18} e^{(-12,100/T)}$	-
$\text{NO}^++\text{O}\leftrightarrow \text{NO}+\text{O}^+$	$2.75 \times 10^{15} T^{-0.01} e^{(-51,000/T)}$	-
$\text{N}_2+\text{O}^+\leftrightarrow \text{N}_2^++\text{O}$	$6.33 \times 10^{13} T^{-0.21} e^{(-22,200/T)}$	-
$\text{NO}^++\text{O}_2\leftrightarrow \text{NO}+\text{O}_2^+$	$1.03 \times 10^{16} T^{-0.17} e^{(-32,400/T)}$	-
$\text{NO}^++\text{N}\leftrightarrow \text{N}_2^++\text{O}$	$1.70 \times 10^{13} T^{-0.40} e^{(-35,500/T)}$	-
$\text{N}+\text{O}\leftrightarrow \text{NO}^++\text{e}^-$	$1.53 \times 10^9 T^{0.37} e^{(-32,000/T)}$	-
$2\text{O}\leftrightarrow \text{O}_2^++\text{e}^-$	$3.85 \times 10^9 T^{0.49} e^{(-80,600/T)}$	-
$2\text{N}\leftrightarrow \text{N}_2^++\text{e}^-$	$1.79 \times 10^9 T^{0.77} e^{(-67,500/T)}$	-
$\text{O}+\text{e}^-\leftrightarrow \text{O}^++2\text{e}^-$	$3.90 \times 10^{33} T^{-3.78} e^{(-158,500/T)}$	-
$\text{N}+\text{e}^-\leftrightarrow \text{N}^++2\text{e}^-$	$2.50 \times 10^{33} T^{-3.82} e^{(-168,600/T)}$	-

Table 8 presents the forward coefficients of the chemical reactions. The B_1, B_2, B_3, B_4 and B_5 constants are presented in Tab. 9 for each reaction.

Table 9. Chemical reactions and equilibrium constant coefficients.

Reaction	B_1	B_2	B_3	B_4	B_5
$\text{O}_2+\text{M}\leftrightarrow 2\text{O}+\text{M}$	2.885	0.988	-6.181	-0.023	-0.001
$\text{N}_2+\text{N}\leftrightarrow 2\text{N}+\text{N}$	1.858	-1.325	-9.856	-0.174	0.008
$\text{N}_2+\text{O}\leftrightarrow 2\text{N}+\text{O}$	1.858	-1.325	-9.856	-0.174	0.008
$\text{N}_2+\text{M}\leftrightarrow 2\text{N}+\text{M}$	1.858	-1.325	-9.856	-0.174	0.008
$\text{N}_2+\text{NO}\leftrightarrow 2\text{N}+\text{NO}$	1.858	-1.325	-9.856	-0.174	0.008
$\text{NO}+\text{M}\leftrightarrow \text{N}+\text{O}+\text{M}$	0.792	-0.492	-6.761	-0.091	0.004
$\text{NO}+\text{O}\leftrightarrow \text{O}_2+\text{N}$	-2.063	-1.480	-0.580	-0.114	0.005
$\text{N}_2+\text{O}\leftrightarrow \text{NO}+\text{N}$	1.066	-0.833	-3.095	-0.084	0.004
$\text{O}_2^++\text{O}\leftrightarrow \text{O}_2+\text{O}^+$	-0.276	0.888	-2.180	0.055	-0.003
$\text{N}_2+\text{N}^+\leftrightarrow \text{N}_2^++\text{N}$	0.307	-1.076	-0.878	-0.004	-0.001
$\text{NO}^++\text{O}\leftrightarrow \text{NO}+\text{O}^+$	0.148	-1.011	-4.121	-0.132	0.006
$\text{N}_2+\text{O}^+\leftrightarrow \text{N}_2^++\text{O}$	2.979	0.382	-3.237	0.168	-0.009
$\text{NO}^++\text{O}_2\leftrightarrow \text{NO}+\text{O}_2^+$	0.424	-1.098	-1.941	-0.187	0.009
$\text{NO}^++\text{N}\leftrightarrow \text{N}_2^++\text{O}$	2.061	0.204	-4.263	0.119	-0.006
$\text{N}+\text{O}\leftrightarrow \text{NO}^++\text{e}^-$	-7.053	-0.532	-4.429	0.150	-0.007
$2\text{O}\leftrightarrow \text{O}_2^++\text{e}^-$	-8.692	-3.110	-6.950	-0.151	0.007
$2\text{N}\leftrightarrow \text{N}_2^++\text{e}^-$	-4.992	-0.328	-8.693	0.269	-0.013
$\text{O}+\text{e}^-\leftrightarrow \text{O}^++2\text{e}^-$	-6.113	-2.035	-15.311	-0.073	0.004
$\text{N}+\text{e}^-\leftrightarrow \text{N}^++2\text{e}^-$	-3.441	-0.577	-17.671	0.099	-0.005

6 Vibrational Model

The vibrational internal energy of a molecule, in J/kg, is defined by:

$$e_{v,s} = \frac{R_s \theta_{v,s}}{e^{\theta_{v,s}/T_v} - 1}, \quad (52)$$

obtained by the integration of Eq. (20), and the vibrational internal energy of all molecules is given by:

$$e_v = \sum_{s=\text{mol}} c_s e_{v,s}. \quad (53)$$

The heat flux due to translational-vibrational relaxation, according to [31], is given by:

$$q_{T-v,s} = \rho_s \frac{e_{v,s}^*(T) - e_{v,s}(T_v)}{\tau_s}, \quad (54)$$

where: $e_{v,s}^*$ is the vibrational internal energy calculated at the translational temperature to the species “s”; and τ_s is the translational-vibrational relaxation time to the molecular species, in s. The relaxation time is the time of energy exchange between the translational and vibrational molecular modes.

6.1. Vibrational characteristic time of Millikan and White

According to [32], the relaxation time of molar average of [33] is described by:

$$\tau_s = \tau_s^{M-W} = \sum_{l=1}^{ns} X_l / \sum_{l=1}^{ns} X_l / \tau_{s,l}^{M-W}, \quad (55)$$

with:

$\tau_{s,l}^{M-W}$ is the relaxation time between species of [33];

τ_s^{M-W} is the vibrational characteristic time of [33];

$$X_l = c_l / (N_{AV} m_l) \quad \text{and} \quad m_l = M_l / N_{AV}. \quad (56)$$

6.2. Definition of $\tau_{s,l}^{M-W}$:

For temperatures inferior to or equal to 8,000 K, [33] give the following semi-empirical correlation to the vibrational relaxation time due to inelastic collisions:

$$\tau_{s,l}^{M-W} = \left(\frac{B}{p_l} \right) e^{[A_{s,l}(T^{-1/3} - 0.015\mu_{s,l}^{1/4}) - 18.42]}, \quad (57)$$

where:

$$B = 1.013 \times 10^5 \text{Ns/m}^2 \quad ([34]);$$

p_l is the partial pressure of species “l” in N/m²;

$$A_{s,l} = 1.16 \times 10^{-3} \mu_{s,l}^{1/2} \theta_{v,s}^{4/3} \quad ([34]); \quad (58)$$

$$\mu_{s,l} = \frac{M_s M_l}{M_s + M_l}, \quad (59)$$

being the reduced molecular mass of the collision partners: kg/kg-mol;

T and $\theta_{v,s}$ in Kelvin.

6.3. Park’s correction time

For temperatures superiors to 8,000 K, the Eq. (57) gives relaxation times less than those observed in experiments. To temperatures above 8,000 K, [28] suggests the following relation to the vibrational relaxation time:

$$\tau_s^P = \frac{1}{\xi_s \sigma_v n_s}, \quad (60)$$

where:

$$\xi_s = \sqrt{\frac{8R_s T}{\pi}}, \quad (61)$$

being the molecular average velocity in m/s;

$$\sigma_v = 10^{-20} \left(\frac{50,000}{T} \right)^2, \quad (62)$$

being the effective collision cross-section to vibrational relaxation in m²; and

$$n_s = \rho_s / m_s, \quad (63)$$

being the density of the number of collision particles of species “s”. ρ_s in kg/m³ and m_s in kg/particle, defined by Eq. (56).

Combining the two relations, the following expression to the vibrational relaxation time is obtained:

$$\tau_s = \tau_s^{M-W} + \tau_s^P. \quad (64)$$

[28] emphasizes that this expression [Eq. (64)] to the vibrational relaxation time is applicable to a range of temperatures much more vast.

6.4. Vibrational/electronic source terms

First of all, one needs to determine the electronic energy of atoms and molecules. This energy is taken into account considering the degeneracies and the electronic characteristic temperature. Such terms are described as follows:

$$e_{el,s} = R_s \frac{\sum_{i=1}^{nd} g_{s,i} \bar{\theta}_{s,i} e^{-\bar{\theta}_{s,i}/T_v}}{\sum_{i=0}^{nd} g_{s,i} e^{-\bar{\theta}_{s,i}/T_v}} \quad (65)$$

where “s” defines a molecular species. The non-preferential mode to create or destroyer a molecular system is defined by:

$$D_{v,s} = \dot{\omega}_s (e_{v,s} + e_{el,s}). \quad (66)$$

The preferential mode is determined by:

$$D_{v,s} = \dot{\omega}_s (\hat{c}_1 \times D_d + e_{el,s}) \quad (67)$$

where the molecular dissociation potential D_d assumes the following values:

Table 10. Dissociation potential.

Species	D_d
N_2	3.36×10^7
O_2	1.54×10^7
NO	2.09×10^7
N_2^+	3.00×10^7
O_2^+	2.01×10^7
NO^+	3.49×10^7

The \hat{c}_1 parameter assumes a typical value of 0.3. The third source term is due to electron work, defined by:

$$T_{pr} = pr(e^-) \times \left(\frac{\partial u}{\partial x} + \frac{\partial v}{\partial y} \right) \quad (68)$$

The fourth term is due to electron impact ionization, considering the ionization reactions involving electrons. These equations are defined by:



This term is specified considering the forward reaction rate coefficients of such reactions. Hence,

$$T_{ion} = np_{e1} I(N) + np_{e2} I(O) \quad (69)$$

with np_{e1} and np_{e2} representing the forward reaction rate coefficients and $I(N)$ and $I(O)$ are the ionization potentials of each species. The value of $I(N)$ is 1.40×10^9 and of $I(O)$ is 1.31×10^9 . The forward reaction rate coefficients are calculated with the vibrational / electronic temperature. The resulting source term is thereafter calculated by the following expression:

$$S_v = \sum_{s=mol} q_{T-v,s} + \sum_{s=mol} D_{v,s} - T_{pr} - T_{ion} \quad (70)$$

The incomplete eleven species model considers only the two sums in the above equation.

7 Numerical Algorithms

7.1 Structured algorithms

The approximation of the integral equation (1) to a rectangular finite volume yields a system of ordinary differential equations with respect to time:

$$V_{i,j} dQ_{i,j}/dt = -C_{i,j}, \quad (71)$$

with $C_{i,j}$ representing the net flux (residue) of conservation of mass, of linear momentum, of total energy, of species mass conservation, and of vibrational energy in the $V_{i,j}$ volume. The cell volume is defined by:

$$V_{i,j} = 0.5 \left[(x_{i,j} - x_{i+1,j}) y_{i+1,j+1} + (x_{i+1,j} - x_{i+1,j+1}) y_{i,j} + (x_{i+1,j+1} - x_{i,j}) y_{i+1,j} \right] + 0.5 \left[(x_{i,j} - x_{i+1,j+1}) y_{i,j+1} + (x_{i+1,j+1} - x_{i,j+1}) y_{i,j} + (x_{i,j+1} - x_{i,j}) y_{i+1,j+1} \right], \quad (72)$$

where a structured computational cell, its nodes and flux surfaces are defined in Fig. 1.

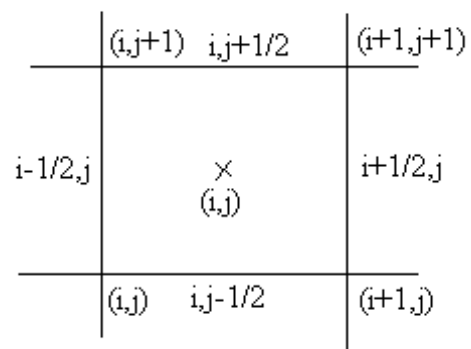


Figure 1. Structured computational cell.

As shown in [24], the discrete convective flux calculated by the AUSM scheme (“Advection Upstream Splitting Method”) can be interpreted as a sum involving the arithmetical average between the right (R) and the left (L) states of the $(i+1/2,j)$ cell face, related to cell (i,j) and its $(i+1,j)$ neighbour, respectively, multiplied by the interface Mach number, and a scalar dissipative term. [35] have suggested that the flux integrals could be calculated defining each part, dynamic, chemical and vibrational, separately. Hence, to the $(i+1/2,j)$ interface, considering the dynamical part of the formulation:

$$R_{i+1/2,j} = |S|_{i+1/2,j} \left\{ \frac{1}{2} M_{i+1/2,j} \left[\begin{pmatrix} \rho a \\ \rho a u \\ \rho a v \\ \rho a H \end{pmatrix}_L + \begin{pmatrix} \rho a \\ \rho a u \\ \rho a v \\ \rho a H \end{pmatrix}_R \right] \right\} \quad (73a)$$

$$-\frac{1}{2}\phi_{i+1/2,j} \left[\begin{array}{c} \left(\begin{array}{c} \rho a \\ \rho a u \\ \rho a v \\ \rho a H \end{array} \right)_R - \left(\begin{array}{c} \rho a \\ \rho a u \\ \rho a v \\ \rho a H \end{array} \right)_L \end{array} \right] + \begin{array}{c} \left(\begin{array}{c} 0 \\ S_x p \\ S_y p \\ 0 \end{array} \right)_{i+1/2,j} \end{array} . \quad (73b)$$

The components of the unity vector normal to the flux interface and the area of the flux interface “I”, n_x^1 , n_y^1 and S^1 , are defined as:

$$\begin{aligned} n_x^1 &= \Delta y_1 / (\Delta x_1^2 + \Delta y_1^2)^{0.5}, \\ n_y^1 &= -\Delta x_1 / (\Delta x_1^2 + \Delta y_1^2)^{0.5}, \\ S^1 &= (\Delta x_1^2 + \Delta y_1^2)^{0.5}. \end{aligned} \quad (74)$$

Expressions to Δx_1 and Δy_1 are given in Tab. 11. The area components are obtained by the product of the respective normal vector component and the area S.

Table 11. Values of Δx_1 and Δy_1 to the structured case.

Interface	Δx_1	Δy_1
$l = (i,j-1/2)$	$x_{i+1,j} - x_{i,j}$	$y_{i+1,j} - y_{i,j}$
$l = (i+1/2,j)$	$x_{i+1,j+1} - x_{i+1,j}$	$y_{i+1,j+1} - y_{i+1,j}$
$l = (i,j+1/2)$	$x_{i,j+1} - x_{i+1,j+1}$	$y_{i,j+1} - y_{i+1,j+1}$
$l = (i-1/2,j)$	$x_{i,j} - x_{i,j+1}$	$y_{i,j} - y_{i,j+1}$

The “a” quantity represents the frozen speed of sound. $M_{i+1/2,j}$ defines the advection Mach number at the $(i+1/2,j)$ face of the (i,j) cell, which is calculated according to [24] as:

$$M_l = M_L^+ + M_R^-, \quad (75)$$

where the separated Mach numbers $M^{+/-}$ are defined by the [23] formulas:

$$\begin{aligned} M^+ &= \begin{cases} M, & \text{if } M \geq 1; \\ 0.25(M+1)^2, & \text{if } |M| < 1; \\ 0, & \text{if } M \leq -1; \end{cases} \\ M^- &= \begin{cases} 0, & \text{if } M \geq 1; \\ -0.25(M-1)^2, & \text{if } |M| < 1; \\ M, & \text{if } M \leq -1. \end{cases} \end{aligned} \quad (76)$$

M_L and M_R represent the Mach number associated with the left and right states, respectively. The advection Mach number is defined by:

$$M = (S_x u + S_y v) / (|S| a). \quad (77)$$

The pressure at the $(i+1/2,j)$ face of the (i,j) cell is calculated by a similar way:

$$p_l = p_L^+ + p_R^-, \quad (78)$$

with $p^{+/-}$ denoting the pressure separation defined according to the [23] formulas:

$$\begin{aligned} p^+ &= \begin{cases} p, & \text{if } M \geq 1; \\ 0.25p(M+1)^2(2-M), & \text{if } |M| < 1; \\ 0, & \text{if } M \leq -1; \end{cases} \\ p^- &= \begin{cases} 0, & \text{if } M \geq 1; \\ 0.25p(M-1)^2(2+M), & \text{if } |M| < 1; \\ p, & \text{if } M \leq -1. \end{cases} \end{aligned} \quad (79)$$

The definition of the dissipative term ϕ determines the particular formulation of the convective fluxes. According to [36], the choice below corresponds to the [23] scheme:

$$\phi_{i+1/2,j} = \begin{cases} |M_{i+1/2,j}|, & \text{if } |M_{i+1/2,j}| \geq 1; \\ |M_{i+1/2,j}| + 0.5(M_R - 1)^2, & \text{if } 0 \leq M_{i+1/2,j} < 1; \\ |M_{i+1/2,j}| + 0.5(M_L + 1)^2, & \text{if } -1 < M_{i+1/2,j} \leq 0; \end{cases} \quad (80)$$

and the choice below corresponds to the [24] scheme:

$$\phi_{i+1/2,j} = |M_{i+1/2,j}|; \quad (81)$$

the discrete-chemical-convective flux, to an eleven species chemical model, is defined by:

$$R_{i+1/2,j} = |S_{i+1/2,j}| \left\{ \frac{1}{2} M_{i+1/2,j} \left[\begin{array}{c} \left(\begin{array}{c} \rho_1 a \\ \rho_2 a \\ \rho_4 a \\ \rho_5 a \\ \rho_6 a \\ \rho_7 a \\ \rho_8 a \\ \rho_9 a \\ \rho_{10} a \\ \rho_{11} a \end{array} \right)_L \left(\begin{array}{c} \rho_1 a \\ \rho_2 a \\ \rho_4 a \\ \rho_5 a \\ \rho_6 a \\ \rho_7 a \\ \rho_8 a \\ \rho_9 a \\ \rho_{10} a \\ \rho_{11} a \end{array} \right)_R \end{array} \right] + \frac{1}{2} \phi_{i+1/2,j} \left[\begin{array}{c} \left(\begin{array}{c} \rho_1 a \\ \rho_2 a \\ \rho_4 a \\ \rho_5 a \\ \rho_6 a \\ \rho_7 a \\ \rho_8 a \\ \rho_9 a \\ \rho_{10} a \\ \rho_{11} a \end{array} \right)_R \left(\begin{array}{c} \rho_1 a \\ \rho_2 a \\ \rho_4 a \\ \rho_5 a \\ \rho_6 a \\ \rho_7 a \\ \rho_8 a \\ \rho_9 a \\ \rho_{10} a \\ \rho_{11} a \end{array} \right)_L \end{array} \right] \right\} \quad (82)$$

and the discrete-vibrational-convective flux is determined by:

$$R_{i+1/2,j} = |S|_{i+1/2,j} \left\{ \frac{1}{2} M_{i+1/2,j} [(\rho e_v a)_L + (\rho e_v a)_R] - \frac{1}{2} \phi_{i+1/2,j} [(\rho e_v a)_R - (\rho e_v a)_L] \right\}. \quad (83)$$

The time integration is performed employing the Runge-Kutta explicit method of five stages, second-order accurate, to the three types of convective flux. To the dynamic part, this method can be represented in general form by:

$$\begin{aligned} Q_{i,j}^{(0)} &= Q_{i,j}^{(n)} \\ Q_{i,j}^{(k)} &= Q_{i,j}^{(0)} - \alpha_k \Delta t_{i,j} R(Q_{i,j}^{(k-1)})/V_{i,j}, \quad (84) \\ Q_{i,j}^{(n+1)} &= Q_{i,j}^{(k)} \end{aligned}$$

to the chemical part, it can be represented in general form by:

$$\begin{aligned} Q_{i,j}^{(0)} &= Q_{i,j}^{(n)} \\ Q_{i,j}^{(k)} &= Q_{i,j}^{(0)} - \alpha_k \Delta t_{i,j} [R(Q_{i,j}^{(k-1)})/V_{i,j} - S_C(Q_{i,j}^{(k-1)})], \\ Q_{i,j}^{(n+1)} &= Q_{i,j}^{(k)} \end{aligned} \quad (85)$$

where the chemical source term S_C is calculated with the temperature T_{trc} . Finally, to the vibrational part:

$$\begin{aligned} Q_{i,j}^{(0)} &= Q_{i,j}^{(n)} \\ Q_{i,j}^{(k)} &= Q_{i,j}^{(0)} - \alpha_k \Delta t_{i,j} [R(Q_{i,j}^{(k-1)})/V_{i,j} - S_v(Q_{i,j}^{(k-1)})], \\ Q_{i,j}^{(n+1)} &= Q_{i,j}^{(k)} \end{aligned} \quad (86)$$

in which:

$$S_v = \sum_{s=mol} q_{T-v,s} + \sum_{s=mol} S_{C,s} e_{v,s}, \quad (87)$$

for the incomplete model; and according to Eq. (70) for the complete model. The Runge-Kutta method uses $k = 1, \dots, 5$; $\alpha_1 = 1/4$, $\alpha_2 = 1/6$, $\alpha_3 = 3/8$, $\alpha_4 = 1/2$ and $\alpha_5 = 1$. This scheme is first-order accurate in space and second-order accurate in time. The second-order of spatial accuracy is obtained by the ‘‘MUSCL’’ procedure.

The viscous formulation follows that of [37], which adopt the Green theorem to calculate primitive variable gradients. The viscous vectors are obtained by arithmetical average between cell (i,j) and its neighbours. As was done with the convective terms, there is a need to separate the viscous flux in three parts: dynamical viscous flux, chemical viscous flux and vibrational viscous flux. The dynamical part corresponds to the first four equations of the Navier-Stokes ones, the chemical part corresponds to the following ten equations and the vibrational part corresponds to the last equation.

7.2 Unstructured algorithms

The cell volume on an unstructured context is defined by:

$$V_i = 0.5[(x_{n1}y_{n2} + y_{n1}x_{n3} + x_{n2}y_{n3}) - (x_{n3}y_{n2} + y_{n3}x_{n1} + x_{n2}y_{n1})], \quad (88)$$

with n_1 , n_2 and n_3 being the nodes of a given triangular cell. The description of the computational cell and its nodes, flux interfaces and neighbors are shown in Fig. 2.

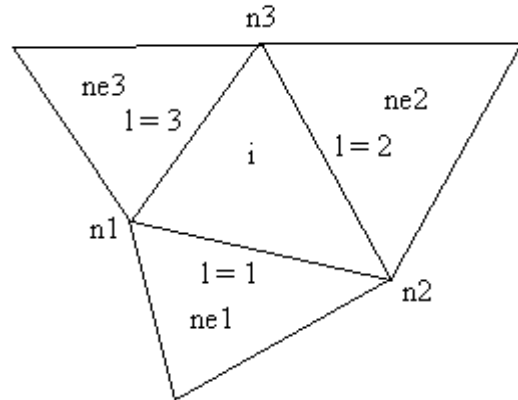


Figure 2. Unstructured computational cell.

The area components at the ‘‘I’’ interface are defined by:

$$S_x^1 = n_x^1 S^1 \quad \text{and} \quad S_y^1 = n_y^1 S^1, \quad (89)$$

where n_x^1 , n_y^1 and S^1 are defined as:

$$\begin{aligned} n_x^1 &= \Delta y_1 / (\Delta x_1^2 + \Delta y_1^2)^{0.5}, \\ n_y^1 &= -\Delta x_1 / (\Delta x_1^2 + \Delta y_1^2)^{0.5}; \\ S^1 &= (\Delta x_1^2 + \Delta y_1^2)^{0.5}. \end{aligned} \quad (90)$$

Table 12. Values of Δx_i and Δy_i .

Interface	Δx_i	Δy_i
1 = 1	$x_{n2} - x_{n1}$	$y_{n2} - y_{n1}$
1 = 2	$x_{n3} - x_{n2}$	$y_{n3} - y_{n2}$
1 = 3	$x_{n1} - x_{n3}$	$y_{n1} - y_{n3}$

Expressions to Δx_i and Δy_i are given in Tab. 12. Considering the two-dimensional and unstructured case, the algorithm follows that described in section 7.1. Hence, the discrete-dynamic-convective flux is defined by:

$$R_1 = |S_1| \left\{ \frac{1}{2} M_1 \left[\begin{array}{c} \left(\begin{array}{c} \rho a \\ \rho a u \\ \rho a v \\ \rho a H \end{array} \right)_L \\ + \\ \left(\begin{array}{c} \rho a \\ \rho a u \\ \rho a v \\ \rho a H \end{array} \right)_R \end{array} \right] - \frac{1}{2} \phi_1 \left[\begin{array}{c} \left(\begin{array}{c} \rho a \\ \rho a u \\ \rho a v \\ \rho a H \end{array} \right)_R \\ - \\ \left(\begin{array}{c} \rho a \\ \rho a u \\ \rho a v \\ \rho a H \end{array} \right)_L \end{array} \right] \right\} + \begin{array}{c} \left(\begin{array}{c} 0 \\ S_x p \\ S_y p \\ 0 \end{array} \right)_1 \end{array}, \quad (91)$$

the discrete-chemical-convective flux is defined by:

$$R_1 = |S_1| \left\{ \frac{1}{2} M_1 \left[\begin{array}{c} \left(\begin{array}{c} \rho_1 a \\ \rho_2 a \\ \rho_4 a \\ \rho_5 a \\ \rho_6 a \\ \rho_7 a \\ \rho_8 a \\ \rho_9 a \\ \rho_{10} a \\ \rho_{11} a \end{array} \right)_L \\ + \\ \left(\begin{array}{c} \rho_1 a \\ \rho_2 a \\ \rho_4 a \\ \rho_5 a \\ \rho_6 a \\ \rho_7 a \\ \rho_8 a \\ \rho_9 a \\ \rho_{10} a \\ \rho_{11} a \end{array} \right)_R \end{array} \right] - \frac{1}{2} \phi_1 \left[\begin{array}{c} \left(\begin{array}{c} \rho_1 a \\ \rho_2 a \\ \rho_4 a \\ \rho_5 a \\ \rho_6 a \\ \rho_7 a \\ \rho_8 a \\ \rho_9 a \\ \rho_{10} a \\ \rho_{11} a \end{array} \right)_R \\ - \\ \left(\begin{array}{c} \rho_1 a \\ \rho_2 a \\ \rho_4 a \\ \rho_5 a \\ \rho_6 a \\ \rho_7 a \\ \rho_8 a \\ \rho_9 a \\ \rho_{10} a \\ \rho_{11} a \end{array} \right)_L \end{array} \right] \right\}, \quad (92)$$

and the discrete-vibrational-convective flux is determined by:

$$R_1 = |S_1| \left\{ \frac{1}{2} M_1 \left[\left(\rho e_v a \right)_L + \left(\rho e_v a \right)_R \right] - \frac{1}{2} \phi_1 \left[\left(\rho e_v a \right)_R - \left(\rho e_v a \right)_L \right] \right\}. \quad (93)$$

The time integration is performed employing the Runge-Kutta explicit method of five stages, second-order accurate, to the three types of convective flux.

To the dynamical part, this method can be represented in general form by:

$$\begin{aligned} Q_i^{(0)} &= Q_i^{(n)} \\ Q_i^{(k)} &= Q_i^{(0)} - \alpha_k \Delta t_i \left[R(Q_i^{(k-1)}) / V_i \right], \quad (94) \\ Q_i^{(n+1)} &= Q_i^{(k)} \end{aligned}$$

to the chemical part, it can be represented in general form by:

$$\begin{aligned} Q_i^{(0)} &= Q_i^{(n)} \\ Q_i^{(k)} &= Q_i^{(0)} - \alpha_k \Delta t_i \left[R(Q_i^{(k-1)}) / V_i - S_C(Q_i^{(k-1)}) \right], \quad (95) \\ Q_i^{(n+1)} &= Q_i^{(k)} \end{aligned}$$

where the chemical source term S_C is calculated with the temperature T_{trc} . Finally, to the vibrational part:

$$\begin{aligned} Q_i^{(0)} &= Q_i^{(n)} \\ Q_i^{(k)} &= Q_i^{(0)} - \alpha_k \Delta t_i \left[R(Q_i^{(k-1)}) / V_i - S_v(Q_i^{(k-1)}) \right], \quad (96) \\ Q_i^{(n+1)} &= Q_i^{(k)} \end{aligned}$$

in which:

$$S_v = \sum_{s=mol} q_{T-v,s} + \sum_{s=mol} S_{C,s} e_{v,s}; \quad (97)$$

for the incomplete model; and according to Eq. (70) for the complete model. The Runge-Kutta method uses $k = 1, \dots, 5$; $\alpha_1 = 1/4$, $\alpha_2 = 1/6$, $\alpha_3 = 3/8$, $\alpha_4 = 1/2$ and $\alpha_5 = 1$. This scheme is first-order accurate in space and second-order accurate in time.

8 MUSCL Approach

Second order spatial accuracy can be achieved by introducing more upwind points or cells in the schemes. It has been noted that the projection stage, whereby the solution is projected in each cell face ($i-1/2, j$; $i+1/2, j$) on piecewise constant states, is the cause of the first order spatial accuracy of the Godunov schemes ([38]). Hence, it is sufficient to modify the first projection stage without modifying the Riemann solver, in order to generate higher spatial approximations. The state variables at the interfaces are thereby obtained from an extrapolation between neighboring cell averages. This method for the generation of second order upwind schemes based on variable extrapolation is often referred to in the literature as the MUSCL ("Monotone Upstream-centered Schemes for

Conservation Laws”) approach. The use of nonlinear limiters in such procedure, with the intention of restricting the amplitude of the gradients appearing in the solution, avoiding thus the formation of new extrema, allows that first order upwind schemes be transformed in TVD (“Total Variation Diminishing”) high resolution schemes with the appropriate definition of such nonlinear limiters, assuring monotone preserving and total variation diminishing methods. Details of the present implementation of the MUSCL procedure, as well the incorporation of TVD properties to the schemes, are found in [38]. The expressions to calculate the fluxes following a MUSCL procedure and the nonlinear flux limiter definitions employed in this work, which incorporates TVD properties, are defined as follows.

The conserved variables at the interface (i+1/2,j) can be considered as resulting from a combination of backward and forward extrapolations. To a linear one-sided extrapolation at the interface between the averaged values at the two upstream cells (i,j) and (i+1,j), one has:

$$Q_{i+1/2,j}^L = Q_{i,j} + \frac{\varepsilon}{2}(Q_{i,j} - Q_{i-1,j}), \text{ cell } (i,j); \quad (98)$$

$$Q_{i+1/2,j}^R = Q_{i+1,j} - \frac{\varepsilon}{2}(Q_{i+2,j} - Q_{i+1,j}), \text{ cell } (i+1,j), \quad (99)$$

leading to a second order fully one-sided scheme. If the first order scheme is defined by the numerical flux

$$F_{i+1/2,j} = F(Q_{i,j}, Q_{i+1,j}) \quad (100)$$

the second order space accurate numerical flux is obtained from

$$F_{i+1/2,j}^{(2)} = F(Q_{i+1/2,j}^L, Q_{i+1/2,j}^R). \quad (101)$$

Higher order flux vector splitting methods, such as those studied in this work, are obtained from:

$$F_{i+1/2,j}^{(2)} = F^+(Q_{i+1/2,j}^L) + F^-(Q_{i+1/2,j}^R). \quad (102)$$

All second order upwind schemes necessarily involve at least five mesh points or cells.

To reach high order solutions without oscillations around discontinuities, nonlinear limiters are employed, replacing the term ε in Eqs. (98) and (99) by these limiters, evaluated at the left and at the right states of the flux interface. To define such limiters, it is necessary to calculate the ratio of

consecutive variations of the conserved variables. These ratios are defined as follows:

$$r_{i-1/2,j}^+ = (Q_{i+1,j} - Q_{i,j}) / (Q_{i,j} - Q_{i-1,j}),$$

$$r_{i+1/2,j}^+ = (Q_{i+2,j} - Q_{i+1,j}) / (Q_{i+1,j} - Q_{i,j}), \quad (103)$$

where the nonlinear limiters at the left and at the right states of the flux interface are defined by $\Psi^L = \Psi(r_{i-1/2,j}^+)$ and $\Psi^R = \Psi(1/r_{i+1/2,j}^+)$. In this work, five options of nonlinear limiters were considered to the numerical experiments. These limiters are defined as follows:

$$\Psi_1^{VL}(r_1) = \frac{r_1 + |r_1|}{1 + r_1}, \text{ [39] limiter}; \quad (104)$$

$$\Psi_1^{VA}(r_1) = \frac{r_1 + r_1^2}{1 + r_1^2}, \text{ Van Albada limiter}; \quad (105)$$

$$\Psi_1^{MIN}(r_1) = \text{signal}_1 \text{MAX}(0, \text{MIN}(|r_1|, \text{signal}_1)), \quad (106)$$

minmod limiter;

$$\Psi_1^{SB}(r_1) = \text{MAX}(0, \text{MIN}(2r_1, 1), \text{MIN}(r_1, 2)), \quad (107)$$

“Super Bee” limiter, due to [40];

$$\Psi_1^{\beta-L}(r_1) = \text{MAX}(0, \text{MIN}(\beta r_1, 1), \text{MIN}(r_1, \beta)), \quad (108)$$

β -limiter,

with “l” varying from 1 to 15 (two-dimensional space), signal_l being equal to 1.0 if $r_l \geq 0.0$ and -1.0 otherwise, r_l is the ratio of consecutive variations of the lth conserved variable and β is a parameter assuming values between 1.0 and 2.0, being 1.5 the value assumed in this work.

With the implementation of the numerical flux vectors following this MUSCL procedure, second order spatial accuracy and TVD properties are incorporated in the algorithms.

9 Spatially Variable Time Step

The idea of a spatially variable time step consists in keeping constant a CFL number in the calculation domain and to guarantee time steps appropriated to each mesh region during the convergence process. The spatially variable time step can be defined by:

$$\Delta t_{i,j} = \frac{\text{CFL}(\Delta s)_{i,j}}{(|q| + a_f)_{i,j}}, \quad (109)$$

where CFL is the Courant-Friedrichs-Lewis number to method stability; $(\Delta s)_{i,j}$ is a characteristic length of information transport; and $(|q| + a_f)_{i,j}$ is

the maximum characteristic speed of information transport, where a_f is the frozen speed of sound. The characteristic length of information transport, $(\Delta s)_{i,j}$, can be determined by:

$$(\Delta s)_{i,j} = [\text{MIN}(l_{\text{MIN}}, C_{\text{MIN}})]_{i,j}, \quad (110)$$

where l_{MIN} is the minimum side length which forms a computational cell and C_{MIN} is the minimum distance of centroids among the computational cell and its neighbours. The maximum characteristic speed of information transport is defined by $(|q| + a_f)_{i,j}$, with $q = \sqrt{u^2 + v^2}$.

10 Nondimensionalization, Initial and Boundary Conditions

10.1 Nondimensionalization

The nondimensionalization employed in the reactive case, in two-dimensions, consisted in:

- Constant gas of the “s” species, R_s :
 $R_s = R_{\text{univ}}/M_s$ with R_{univ} assuming the value 1.987 cal/(g-mol.K) and M_s in g/g-mol $\Rightarrow R_s$ in cal/(g.K). Multiplying this value by 4.184×10^3 (conversion to Joules and kilogram) the gas constant pass to be evaluated in J/(kg.K). Hence, as the temperature is nondimensionalized with a_{char} , in m/s, in which:
 $a_{\text{char}} = \sqrt{\gamma p_\infty / \rho_\infty}$, with the freestream properties defined by the simulation flight altitude, R_s pass to be nondimensionalized by a_{char} too;
- Specific heat at constant volume of the “s” species, $C_{v,s}$:
as this parameter is directly proportional to the gas constant of the “s” species, its nondimensionalization is also performed by a_{char} ;
- Enthalpy of the “s” species, h_s and h_s^0 :
nondimensionalized by a_{char}^2 . h_s is given in cal/g-mol, what implies that it should be multiplied by 4.184×10^3 to pass for J/kg. Hence, its nondimensionalization is by a_{char}^2 .
 h_s^0 is given in J/g-mol, which implies that it should be divided by M_s to pass for J/g and multiplied by 10^3 to pass for J/kg. With this procedure, its nondimensionalization is by a_{char}^2 ;
- Translational/rotational temperature, T_{tr} : such variable is nondimensionalized by a_{char} ;

- Vibrational temperature, T_v : such variable is nondimensionalized by a_{char} ;
- Characteristic vibrational temperature of the “s” species, $\theta_{v,s}$: such variable is nondimensionalized by a_{char} ;
- Density of the “s” species and of the mixture, ρ_s and ρ : Both variables are nondimensionalized by ρ_∞ , in kg/m³. Note that the species and mixture initial densities are $\rho_{\text{init},s}$ and ρ_{init} , different from ρ_∞ ;
- Velocity components, u and v : both Cartesian components of velocity are dimensionalized by a_{char} ;
- Molecular viscosity, μ : given in kg/(m.s) and nondimensionalized directly by μ_∞ ;
- Thermal conductivity, k : both translational and rotational thermal conductivities, as also the vibrational thermal conductivity, are given in J/(m.s.K) and nondimensionalized by k_∞ ;
- The diffusion coefficient, D : given in m²/s and nondimensionalized by $a_{\text{char}}^2 dt_{\text{char}}$, in which dt_{char} should be the minor time step calculated at the computational domain at the first iteration;
- Chemical source term, $\dot{\omega}$: nondimensionalized by $\rho_\infty \times 10^{-3} / dt_{\text{char}}$. The 10^{-3} term is necessary to convert from kg/m³ to g/cm³. In the equation of the law of mass action, density terms inside the productory are given in kg/m³. They also should be multiplied by 10^{-3} to pass from kg/m³ to g/cm³;
- Vibrational internal energy, e_v : nondimensionalized by a_{char}^2 ;
- Total energy, e : nondimensionalized by $\rho_\infty a_{\text{char}}^2$;
- Pressure, p : nondimensionalized by $\rho_\infty a_{\text{char}}^2$;
- Relaxation time, τ_s : nondimensionalized by dt_{char} .

10.2 Initial conditions

As initial conditions, the following flow properties are given: ρ_{init} , u_{init} , α , $T_{tr,\text{init}}$, $T_{v,\text{init}}$, $c_s(1)$, $c_s(2)$, $c_s(4)$, $c_s(5)$, $c_s(6)$, $c_s(7)$, $c_s(8)$, $c_s(9)$, $c_s(10)$, and $c_s(11)$ in which: α is the flow attack angle, $T_{tr,\text{init}}$ is the initial translational/rotational temperature, $T_{v,\text{init}}$ is the initial vibrational temperature, “init” is relative to the initial conditions and the c_s 's are initial mass fractions of the N, O, O₂, NO, N⁺, O⁺, N₂⁺, O₂⁺, NO⁺ and e⁻, respectively. Hence, $c_s(3)$ is obtained from Eq. (111). Initially, $T_{v,\text{init}} = T_{tr,\text{init}}$.

$$c_s(3) = 1 - [c_s(1) + c_s(2) + c_s(4) + c_s(5) + c_s(6) + c_s(7) + c_s(8) + c_s(9) + c_s(10) + c_s(11)]. \quad (111)$$

The nondimensional variables which compose the vector of initial conserved variables are determined by: $\rho_{\text{nond}} = \rho_{\text{init}}/\rho_{\infty}$, $u_{\text{nond}} = u_{\text{init}}/a_{\text{char}}$, $v_{\text{nond}} = u_{\text{nond}}/\text{tg}(\alpha)$, $T_{\text{tr,nond}} = T_{\text{tr,init}}/a_{\text{char}}$ and $T_{\text{v,nond}} = T_{\text{v,init}}/a_{\text{char}}$, with $\text{tg}(\alpha)$ being the tangent of the α angle (α is the attack angle). With the species and mixture mass fractions and with the values of the specific heats at constant volume, it is possible to obtain the mixture specific heat at constant volume

$$[C_{v,\text{mixt}} = \sum_{s=1}^{\text{ns}} c_s C_{v,s}].$$

The mixture formation enthalpy is also possible to obtain from the species enthalpy and from the species mass fraction,

$$\text{according to } h^0 = \sum_{s=1}^{\text{ns}} c_s h_s^0.$$

The nondimensionalized internal vibrational energy to each molecular species is obtained by:

$$\begin{aligned} e_{v,\text{nond}N_2} &= R_{N_2} \theta_{v,N_2} / \left\{ e^{[\theta_{v,N_2}/T_{v,\text{nond}}]} - 1 \right\}; \\ e_{v,\text{nond}O_2} &= R_{O_2} \theta_{v,O_2} / \left\{ e^{[\theta_{v,O_2}/T_{v,\text{nond}}]} - 1 \right\}; \\ e_{v,\text{nond}NO} &= R_{NO} \theta_{v,NO} / \left\{ e^{[\theta_{v,NO}/T_{v,\text{nond}}]} - 1 \right\}; \\ e_{v,\text{nond}N_2^+} &= R_{N_2^+} \theta_{v,N_2^+} / \left\{ e^{[\theta_{v,N_2^+}/T_{v,\text{nond}}]} - 1 \right\}; \\ e_{v,\text{nond}O_2^+} &= R_{O_2^+} \theta_{v,O_2^+} / \left\{ e^{[\theta_{v,O_2^+}/T_{v,\text{nond}}]} - 1 \right\}; \\ e_{v,\text{nond}NO^+} &= R_{NO^+} \theta_{v,NO^+} / \left\{ e^{[\theta_{v,NO^+}/T_{v,\text{nond}}]} - 1 \right\}; \end{aligned} \quad (112)$$

The nondimensionalized-total-vibrational energy of the system is determined by:

$$\begin{aligned} e_{v,\text{nond}} &= c_{N_2} e_{v,\text{nond}N_2} + c_{O_2} e_{v,\text{nond}O_2} + c_{NO} e_{v,\text{nond}NO} + \\ &+ c_{N_2^+} e_{v,\text{nond}N_2^+} + c_{O_2^+} e_{v,\text{nond}O_2^+} + c_{NO^+} e_{v,\text{nond}NO^+}. \end{aligned} \quad (113)$$

The nondimensionalized-species-electronic energy of the system is determined by Eq. (65). The total electronic energy is defined by:

$$e_{\text{el}} = \sum_{s=1}^{\text{ns}} c_s e_{\text{el},s}, \quad (114)$$

with “ns” being the number of species. The electron vibrational/electronic energy is defined as

$$e_{v-\text{el},e} = C_{v,e} T_v. \quad (115)$$

Finally, the nondimensionalized total energy is obtained by:

$$\begin{aligned} e_{\text{nond}} &= \rho_{\text{nond}} [C_{v,\text{mixt}} T_{\text{tr,nond}} + h_{\text{mixt}}^0 + e_{v,\text{nond}} + e_{\text{el,nond}} + \\ &0.5(u_{\text{nond}}^2 + v_{\text{nond}}^2)]. \end{aligned} \quad (116)$$

The initial vector of conserved variables is defined to an eleven species chemical model of the following form:

$$Q = \begin{Bmatrix} \rho_{\text{nond}} \\ \rho_{\text{nond}} u_{\text{nond}} \\ \rho_{\text{nond}} v_{\text{nond}} \\ e_{\text{nond}} \\ \rho_{\text{nond}} c_s(1) \\ \rho_{\text{nond}} c_s(2) \\ \rho_{\text{nond}} c_s(4) \\ \rho_{\text{nond}} c_s(5) \\ \rho_{\text{nond}} c_s(6) \\ \rho_{\text{nond}} c_s(7) \\ \rho_{\text{nond}} c_s(8) \\ \rho_{\text{nond}} c_s(9) \\ \rho_{\text{nond}} c_s(10) \\ \rho_{\text{nond}} c_s(11) \\ \rho_{\text{nond}} e_{v,\text{nond}} \end{Bmatrix}. \quad (117)$$

10.3 Boundary conditions to the dynamical part

(a) Dynamical Part:

The boundary conditions are basically of three types: solid wall, entrance and exit. These conditions are implemented in special cells, named ghost cell.

(a.1) Wall condition: To the inviscid case, this condition imposes the flow tangency at the solid wall. This condition is satisfied considering the wall tangent velocity component of the ghost volume as equals to the respective velocity component of its real neighbor cell. At the same way, the wall normal velocity component of the ghost cell is equaled in value, but with opposite signal, to the respective

velocity component of the real neighbor cell. It results in:

$$n_x = \Delta y / \sqrt{\Delta x^2 + \Delta y^2}; \quad (118)$$

$$n_y = -\Delta x / \sqrt{\Delta x^2 + \Delta y^2}; \quad (119)$$

where, for the $(i+1/2, j)$ interface:

$$\Delta x = x_{i+1, j+1} - x_{i+1, j}; \quad (120)$$

$$\Delta y = y_{i+1, j+1} - y_{i+1, j}. \quad (121)$$

Hence, the ghost cell velocity components are written as:

$$u_g = (n_y^2 - n_x^2)u_r - (2n_x n_y)v_r; \quad (122)$$

$$v_g = -(2n_x n_y)u_r + (n_y^2 - n_x^2)v_r, \quad (123)$$

with “g” related with ghost cell and “r” related with real cell. To the viscous case, the boundary condition imposes that the ghost cell velocity components be equal to the real cell velocity components, with the negative signal:

$$u_g = -u_r; \quad (124)$$

$$v_g = -v_r. \quad (125)$$

The pressure gradient normal to the wall is assumed be equal to zero, following an inviscid formulation and according to the boundary layer theory. The same hypothesis is applied to the temperature gradient normal to the wall, considering adiabatic wall. The ghost volume density and pressure are extrapolated from the respective values of the real neighbor volume (zero order extrapolation), with these two conditions. The total energy is obtained by the equation (116).

For the eleven species chemical model, it is necessary to consider the electronic energy of the atoms and molecules, Eq. (65), to calculate the total energy. The vibrational / electronic energy contribution from electron is calculated as:

$$e_{el, e^-} = c_{v, e^-} T_v, \quad (126)$$

and the total vibrational-electronic energy is determined by:

$$e_{v-el} = \sum_{s=mol} c_s e_{v,s} + \sum_{s=1}^{ns} c_s e_{el,s}, \quad (127)$$

where $e_{v,s}$ is obtained from Eq. (111) and the $e_{el,s}$ is obtained from Eq. (65). Note that the electronic energy is considered only in the complete model.

(a.2) Entrance condition:

(a.2.1) Subsonic flow: Three properties are specified and one is extrapolated, based on analysis of information propagation along characteristic directions in the calculation domain ([41]). In other words, three characteristic directions of information propagation point inward the computational domain and should be specified. Only the characteristic direction associated to the “ (q_n-a) ” velocity cannot be specified and should be determined by interior information of the calculation domain. The total energy was the extrapolated variable from the real neighbor volume, to the studied problems. Density and velocity components had their values determined by the initial flow properties.

(a.2.2) Supersonic flow: All variables are fixed with their initial flow values.

(a.3) Exit condition:

(a.3.1) Subsonic flow: Three characteristic directions of information propagation point outward the computational domain and should be extrapolated from interior information ([41]). The characteristic direction associated to the “ (q_n-a) ” velocity should be specified because it penetrates the calculation domain. In this case, the ghost volume’s total energy is specified by its initial value. Density and velocity components are extrapolated.

(a.3.2) Supersonic flow: All variables are extrapolated from the interior domain due to the fact that all four characteristic directions of information propagation of the Euler equations point outward the calculation domain and, with it, nothing can be fixed.

(b) Chemical Part:

The boundary conditions to the chemical part are also of three types: solid wall, entrance and exit.

(b.1) Wall condition: In both inviscid and viscous cases, the non-catalytic wall condition is imposed, which corresponds to a zero order extrapolation of the species density from the neighbor real cells.

(b.2) Entrance condition: In this case, the species densities of each ghost cell are fixed with their initial values (freestream values).

(b.3) Exit condition: In this case, the species densities are extrapolated from the values of the neighbor real cell.

(c) Vibrational Part:

The boundary conditions in the vibrational part are also of three types: solid wall, entrance and exit.

(c.1) Wall condition: In both inviscid and viscous cases, the internal vibrational energy of the ghost cell is extrapolated from the value of its neighbor real cell.

(c.2) Entrance condition: In this case, the internal vibrational energy of each ghost cell is fixed with its initial value (freestream value).

(c.3) Exit condition: In this case, the internal vibrational energy is extrapolated from the value of the neighbor real cell.

11 Configurations

11.1 Computational domain descriptions

(1) Blunt body configuration to Earth reentry problems:

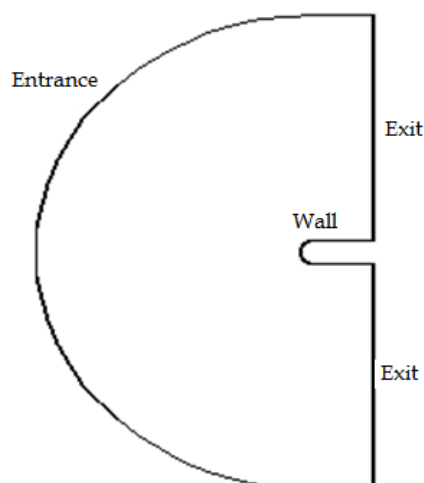


Figure 3. Blunt body physical domain.

Figure 3 presents the computational domain employed in the structured and unstructured simulations in two-dimensions. This figure represents a blunt body with a 1.0 m nose radius and far field located twenty (20) times this radius in relation to the nose configuration. The domain presents three frontiers, as mentioned in the boundary conditions: solid wall, entrance and exit. Such blunt body does not present wall inclination.

Figures 4 and 5 exhibit the employed meshes to the structured and two-dimensional simulations. Figure 4 shows the mesh to the inviscid simulations, whereas figure 5 shows the mesh to the viscous simulations. An exponential stretching of 7.5% in the η direction was employed to the viscous mesh.

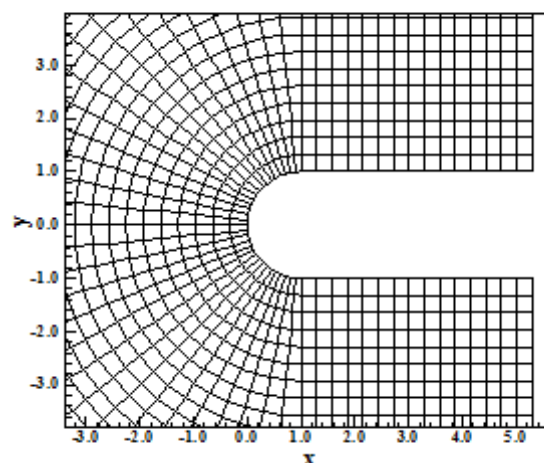


Figure 4. Blunt body inviscid mesh.

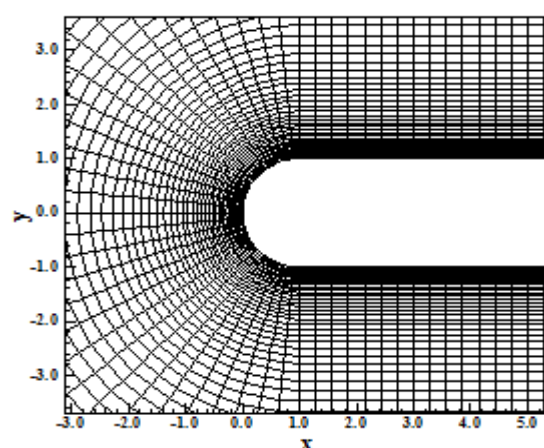


Figure 5. Blunt body viscous mesh.

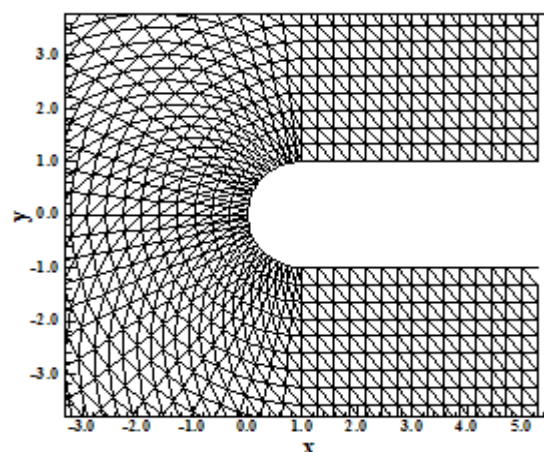


Figure 7. Blunt body inviscid mesh – Same sense.

The inviscid mesh has 3,658 rectangular cells and 3,780 nodes, which corresponds in finite differences to a mesh of 63x60 points. The viscous mesh also has the same number of rectangular cells and nodes, defining again a mesh of 63x60 points.

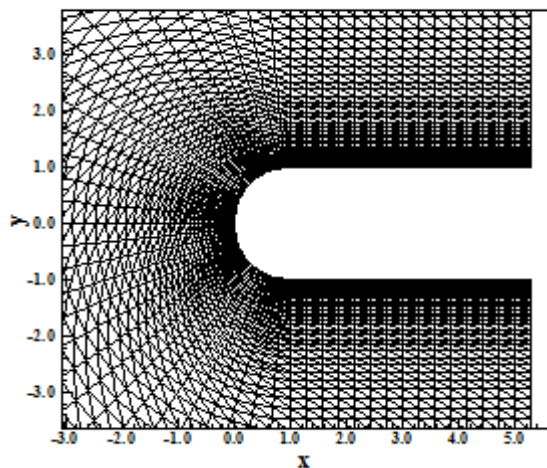


Figure 8. Blunt body viscous mesh – Same sense.

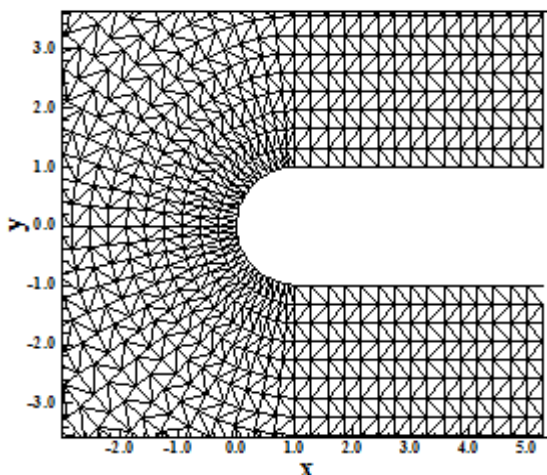


Figure 9. Blunt body inviscid mesh – Alternated sense.

The same meshes employed to the inviscid and viscous structured cases are applied to the unstructured cases. Figures 7 and 8 exhibit the inviscid and viscous unstructured meshes, in the same sense discretization. An exponential stretching of 7.5% in the η direction was also applied. For the unstructured cases, two options of unstructured discretization are possible: the same sense discretization and the alternated sense discretization. As the cells are distributed in the same orientation along the mesh, the discretization is said in the same sense; On the other hand, as the cells are distributed in alternate sense orientations, the discretization is said in the alternated sense. Figures 9 and 10 show the alternated sense discretization option. This form

of orientation of the cells introduces more one line in the mesh, resulting in always using an odd number of lines in the η direction.

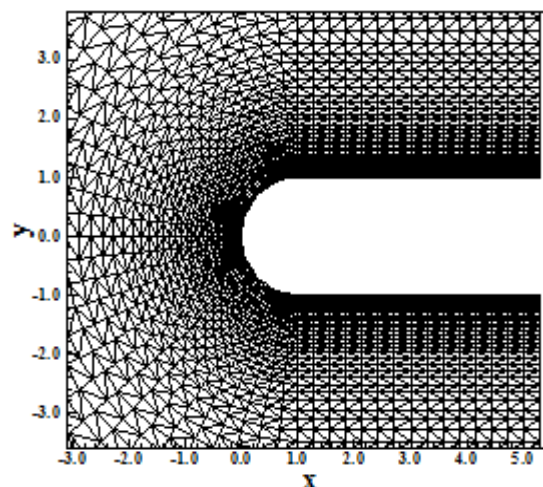


Figure 10. Blunt body viscous mesh – Alternated sense.

(2) Double ellipse configuration:

The double ellipse mesh is composed of 3,528 rectangular cells and 3,650 nodes in the structured case and of 7,056 triangular cells and 3,650 nodes in the unstructured case, for the same sense mesh orientation. The structured mesh has 73x50 points, on a finite difference context. The alternated sense mesh orientation has 73x51 points. An exponential stretching of 7.5% in the η direction was applied to both structured and unstructured configurations.

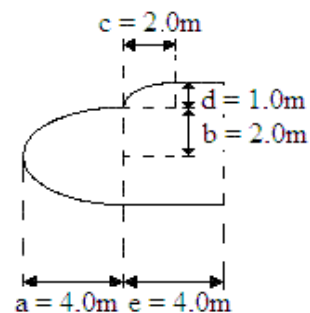


Figure 11. Double ellipse configuration.

Figure 11 exhibits the double ellipse configuration and Figs. 12 and 13 show the structured meshes for the inviscid and viscous cases, respectively. Figures 14 and 15 present the inviscid and viscous unstructured meshes to a same sense orientation, respectively.

Figure 16 and 17 show the inviscid and viscous unstructured meshes to an alternated sense orientation, respectively. The idea of the double ellipse problem is trying to simulate the shuttle flight at the Earth upper atmosphere.

This configuration was also studied in the Mars entry flows ([42-43]), trying to simulate the behaviour of the shuttle in such environment.

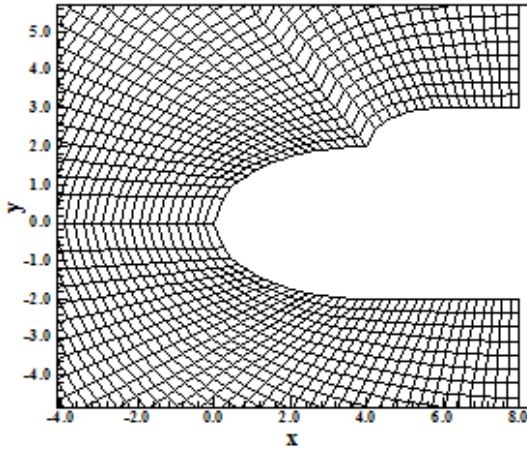


Figure 12. Double ellipse inviscid mesh.

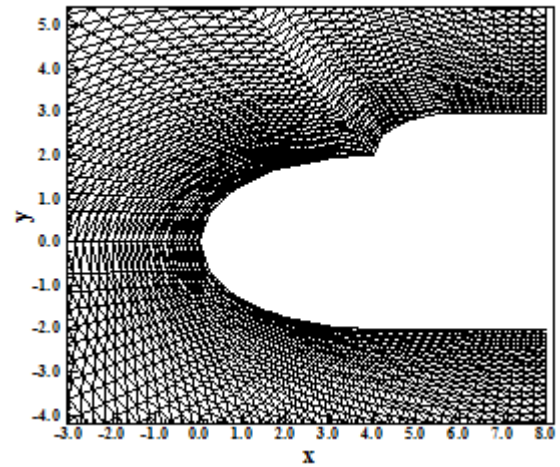


Figure 15. Double ellipse viscous mesh (Same Sense).

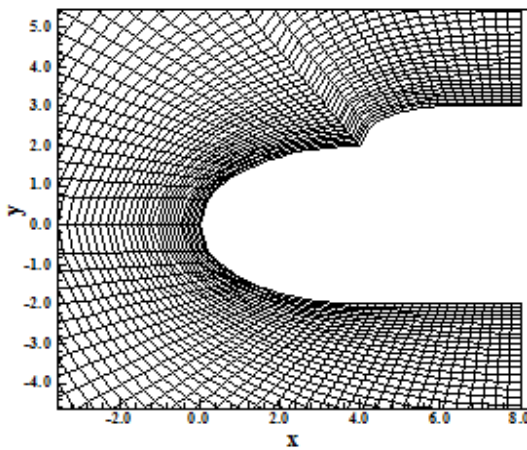


Figure 13. Double ellipse viscous mesh.

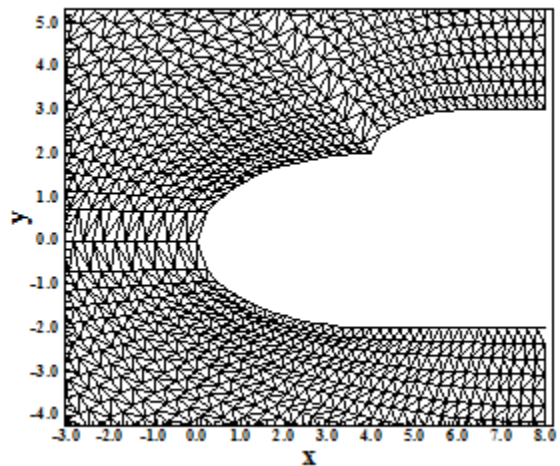


Figure 16. Double ellipse inviscid mesh (Alternated Sense).

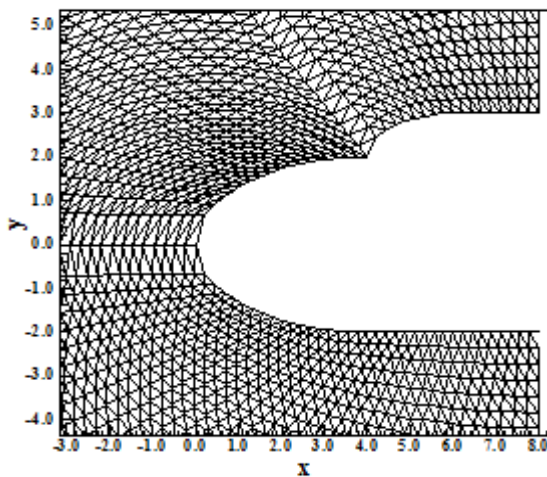


Figure 14. Double ellipse inviscid mesh (Same Sense).

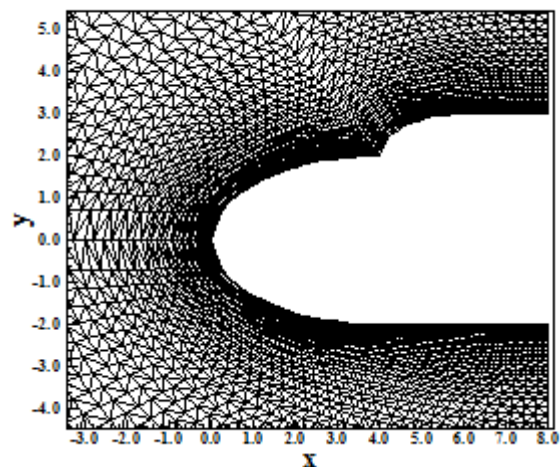


Figure 17. Double ellipse viscous mesh (Alternated Sense).

(3) Reentry capsule configuration:

The reentry capsule is composed of 3,136 rectangular cells and 3,250 nodes in the structured case. This mesh is equivalent in finite differences to a grid of 65x50 points.

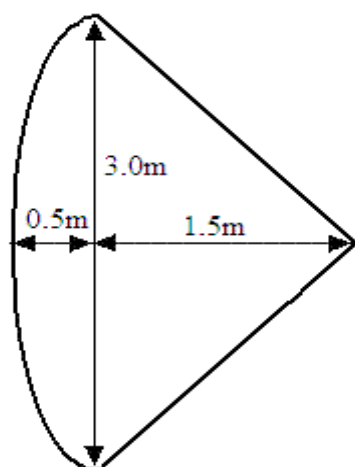


Figure 18. Reentry capsule configuration.

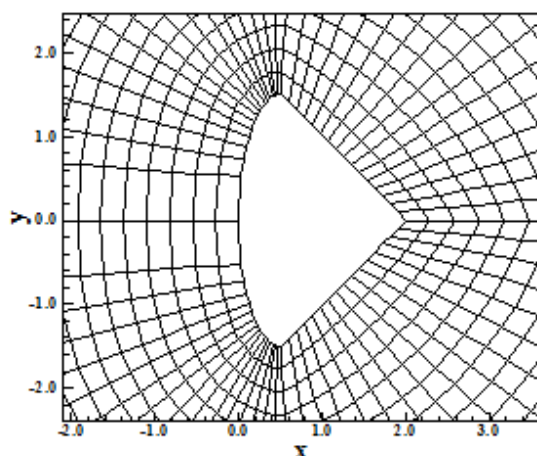


Figure 19. Reentry capsule inviscid mesh.

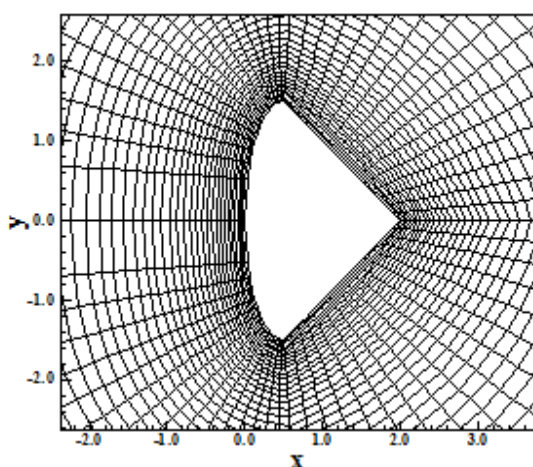


Figure 20. Reentry capsule viscous mesh.

The unstructured case to the reentry capsule problem was not simulated. This geometry has four frontiers: solid wall, entrance, exit and continuity. This last boundary is implemented considering the properties of the flow at the wake upper side as equal to the wake lower side, assuring in this way the conservation of the flow at the wake frontier.

Figure 18 exhibits the reentry capsule configuration. The inviscid and viscous meshes are presented in Figs. 19 and 20.

12 Conclusion

This work, the first part of this study, presents a numerical tool implemented to simulate inviscid and viscous flows employing the reactive gas formulation of thermochemical non-equilibrium flow in two-dimensions. The Euler and Navier-Stokes equations, employing a finite volume formulation, on the context of structured and unstructured spatial discretizations, are solved. These variants allow an effective comparison between the two types of spatial discretization aiming verify their potentialities: solution quality, convergence speed, computational cost, etc. The aerospace problems involving the “hot gas” hypersonic flows around a blunt body, around a double ellipse, and around a reentry capsule in two-dimensions, are simulated.

To the simulations with unstructured spatial discretization, a structured mesh generator developed by the first author ([44]), which creates meshes of quadrilaterals (2D), was employed. After that, as a pre-processing stage ([45]), such meshes were transformed in meshes of triangles. Such procedure aimed to avoid the time which would be waste with the implementation of an unstructured generator, which was not the objective of the present work, and to obtain a generalized algorithm to the solution of the reactive equations.

In this work, first part of this study, the structured and unstructured formulations of the two-dimensional Euler and Navier-Stokes reactive equations are presented. In [46], the second part of this study, it will be presented the structured and unstructured solutions.

The reactive simulations involved an air chemical model of eleven species: N, O, N₂, O₂, NO, N⁺, O⁺, N₂⁺, O₂⁺, NO⁺ and e⁻. Thirty-two or fourth-three chemical reactions, involving dissociation, recombination and ionization, were simulated by the proposed models. In the former case, the [27] model is employed, whereas in the latter, the [28] model was used. The Arrhenius formula was employed to determine the reaction

rates and the law of mass action was used to determine the source terms of each gas species equation.

The results have demonstrated that the most correct aerodynamic coefficient of lift is obtained by the [23] scheme with first-order accuracy, in an inviscid formulation, to the blunt body and reentry capsule problems. The cheapest algorithm was due to [24], inviscid, first-order accurate, and structured discretization. Moreover, the shock position is closer to the geometry as using the reactive formulation than the ideal gas formulation.

Errors less than 20% were obtained with the second-order version of the [23] algorithm in the determination of the stagnation pressure at the body nose, in all three physical problems, and an error around 10% was found in the determination of the shock standoff distance, again in all three physical problems, highlighting the correct implementation and good results obtained from the reactive formulation. Values of these parameters were evaluated and proved the significant potential of the present numerical tool.

References:

- [1] P. A. Gnoffo, R. N. Gupta, and J. L. Shinn, Conservation Equations and Physical Models for Hypersonic Flows in Thermal and Chemical Nonequilibrium, *NASA TP 2867*, 1989.
- [2] M. Liu and M. Vinokur, Upwind Algorithms for General Thermo-Chemical Nonequilibrium Flows, *AIAA Paper 89-0201*, 1989.
- [3] R. N. Gupta, J. M. Yos, R. A. Thompson, and K. -P. Lee, A Review of Reaction Rates and Thermodynamic and Transport Properties for an 11-Species Air Model for Chemical and Thermal Nonequilibrium Calculations to 30000 K, *NASA RP-1232*, 1990.
- [4] R. K. Prabhu, An Implementation of a Chemical and Thermal Nonequilibrium Flow Solver on Unstructured Meshes and Application to Blunt Bodies, *NASA CR-194967*, 1994.
- [5] C. Park, Radiation Enhancement by Nonequilibrium in Earth's Atmosphere, *Journal of Spacecraft and Rockets*, Vol. 22, No. 1, 1985, pp. 27-36.
- [6] C. Park, Problem of Rate Chemistry in the Flight Regimes of Aeroassisted Orbital Transfer Vehicles, *Thermal Design of Aeroassisted Orbital Transfer Vehicles*, Progress in Astronautics and Aeronautics, edited by H. F. Nelson, AIAA, NY, Vol. 96, 1985, pp. 511-537.
- [7] P. A. Gnoffo, Three-Dimensional AOTV Flowfields in Chemical Nonequilibrium, *AIAA Paper 86-0230*, 1986.
- [8] C. P. Li, Implicit Methods for Computing Chemically Reacting Flow, *NASA TM-58274*, 1986.
- [9] J. H. Lee, Basic Governing Equations for the Flight Regimes of Aeroassisted Orbital Transfer Vehicles, *Thermal Design of Aeroassisted Transfer Vehicles*, Progress in Astronautics and Aeronautics, AIAA, Vol. 96, 1985, pp. 3-53.
- [10] C. Park, Convergence of Computation of Chemically Reacting Flows, *Thermophysical Aspects of Re-entry Flows*, Progress in Astronautics and Aeronautics, edited by J. N. Moss and C. D. Scott, AIAA, NY, Vol. 103, pp. 478-513.
- [11] C. Park, Assessment of Two-Temperature Kinetic Model for Dissociating and Weakly-Ionizing Nitrogen, *AIAA Paper 86-1347*, 1986.
- [12] C. Park, Calculation of Nonequilibrium Radiation in the Flight Regimes of Aeroassisted Orbital Transfer Vehicles, *Thermal Design of Aeroassisted Orbital Transfer Vehicles*, Progress in Astronautics and Aeronautics, edited by H. F. Nelson, AIAA, NY, Vol. 96, 1985, pp. 395-418.
- [13] C. Park, Nonequilibrium Air Radiation (NEQAIR) Program: User's Manual, *NASA TM-86707*, 1985.
- [14] R. A. Allen, J. C. Camm, and J. C. Keck, Radiation from Hot Nitrogen, Research Report 102, AVCO-Everett Research Laboratory, Everett, MA, 1961.
- [15] R. A. Allen, J. C. Keck, and J. C. Camm, Nonequilibrium Radiation from Shock Heated Nitrogen and a Determination of the Recombination Rate, Research Report 110, AVCO-Everett Research Laboratory, Everett, MA, 1961.
- [16] R. A. Allen, Nonequilibrium Shock Front Rotational, Vibrational, and Electronic Temperature Measurements, Research Report 186, AVCO-Everett Research Laboratory, Everett, MA, 1964.
- [17] E. S. G. Maciel, and A. P., Pimenta, Thermochemical Non-Equilibrium Reentry Flows in Two-Dimensions – Part I, *Wseas Transactions on Mathematics*, Vol. 11, Issue 6, pp. 520-545.
- [18] E. S. G. Maciel, and A. P., Pimenta, Thermochemical Non-Equilibrium Reentry Flows in Two-Dimensions – Part II, *Wseas*

- Transactions on Mathematics*, Vol. 11, Issue 11, pp. 977-1005.
- [19] S. K. Saxena and M. T. Nair, An Improved Roe Scheme for Real Gas Flow, *AIAA Paper 2005-587*, 2005.
- [20] E. S. G. Maciel, and A. P., Pimenta, Thermochemical Non-Equilibrium Reentry Flows in Two-Dimensions: Seven Species Model – Part I, *Wseas Transactions on Applied and Theoretical Mechanics*, Vol. 7, Issue 4, pp. 311-337.
- [21] E. S. G. Maciel, and A. P., Pimenta, Thermochemical Non-Equilibrium Reentry Flows in Two-Dimensions: Seven Species Model – Part II, *Wseas Transactions on Applied and Theoretical Mechanics*, Vol. 8, Issue 1, pp. 55-83.
- [22] F. G. Blottner, Viscous Shock Layer at the Stagnation Point With Nonequilibrium Air Chemistry, *AIAA Journal*, Vol. 7, No. 12, 1969, pp. 2281-2288.
- [23] B. Van Leer, Flux-Vector Splitting for the Euler Equations, *Lecture Notes in Physics*, Springer Verlag, Berlin, Vol. 170, pp. 507-512, 1982.
- [24] M. Liou, and C. J. Steffen Jr., A New Flux Splitting Scheme, *Journal of Computational Physics*, Vol. 107, 1993, pp. 23-39.
- [25] E. S. G. Maciel, Analysis of Convergence Acceleration Techniques Used in Unstructured Algorithms in the Solution of Aeronautical Problems – Part I, *Proceedings of the XVIII International Congress of Mechanical Engineering (XVIII COBEM)*, Ouro Preto, MG, Brazil, 2005. [CD-ROM]
- [26] E. S. G. Maciel, Analysis of Convergence Acceleration Techniques Used in Unstructured Algorithms in the Solution of Aerospace Problems – Part II, *Proceedings of the XII Brazilian Congress of Thermal Engineering and Sciences (XII ENCIT)*, Belo Horizonte, MG, Brazil, 2008. [CD-ROM]
- [27] M. G. Dunn, and S. W. Kang, Theoretical and Experimental Studies of Reentry Plasmas, *NASA CR-2232*, 1973.
- [28] C. Park, Assessment of Two-Temperature Kinetic Model for Ionizing Air, *Journal of Thermophysics and Heat Transfer*, Vol. 3, No. 13, pp. 233-244, 1989.
- [29] W. G. Vincent and C. H. Kruger Jr., *Introduction to Physical Gas Dynamics*, John Wiley & Sons, Ltd, New York, 1965.
- [30] G. Degrez, and E. Van Der Weide, Upwind Residual Distribution Schemes for Chemical Non-Equilibrium Flows, *AIAA Paper 99-3366*, 1999.
- [31] L. Landau, and E. Teller, Theory of Sound Dispersion, *Physikalische Zeitschrift Der Sowjetunion*, Vol. 10, 1936, pp. 34-43.
- [32] R. Monti, D. Paterna, R. Savino, and A. Esposito, Experimental and Numerical Investigation on Martian Atmosphere Entry, *AIAA Paper 2001-0751*, 2001.
- [33] R. C. Millikan and D. R. White, Systematics of Vibrational Relaxation, *The Journal of Chemical Physics*, Vol. 39, No. 12, 1963, pp. 3209-3213.
- [34] A. F. P. Houwing, S. Nonaka, H. Mizuno, and K. Takayama, Effects of Vibrational Relaxation on Bow Shock Stand-off Distance for Nonequilibrium Flows, *AIAA Journal*, Vol. 38, No. 9, 2000, pp. 1760-1763.
- [35] D. Ait-Ali-Yahia, and W. G. Habashi, Finite Element Adaptive Method for Hypersonic Thermochemical Nonequilibrium Flows, *AIAA Journal* Vol. 35, No. 8, 1997, 1294-1302.
- [36] R. Radespiel, and N. Kroll, Accurate Flux Vector Splitting for Shocks and Shear Layers, *Journal of Computational Physics*, Vol. 121, 1995, pp. 66-78.
- [37] L. N. Long, M. M. S. Khan, and H. T. Sharp, Massively Parallel Three-Dimensional Euler / Navier-Stokes Method, *AIAA Journal*, Vol. 29, No. 5, 1991, pp. 657-666.
- [38] C. Hirsch, Numerical Computation of Internal and External Flows – Computational Methods for Inviscid and Viscous Flows. John Wiley & Sons Ltd, 691p, 1990.
- [39] B. Van Leer, Towards the Ultimate Conservative Difference Scheme. II. Monotonicity and Conservation Combined in a Second-Order Scheme, *Journal of Computational Physics*, Vol. 14, 1974, pp. 361-370.
- [40] P. L. Roe, In *Proceedings of the AMS-SIAM Summer Seminar on Large-Scale Computation in Fluid Mechanics*, Edited by B. E. Engquist et al, *Lectures in Applied Mathematics*, Vol. 22, 1983, p. 163.
- [41] E. S. G. Maciel, Simulação Numérica de Escoamentos Supersônicos e Hipersônicos Utilizando Técnicas de Dinâmica dos Fluidos Computacional, *Doctoral Thesis*, ITA, CTA, São José dos Campos, SP, Brazil, 258p, 2002.
- [42] E. S. G. Maciel, and A. P., Pimenta, Thermochemical Non-Equilibrium Entry Flows in Mars in Two-Dimensions – Part I, *Wseas Transactions on Applied and Theoretical Mechanics*, Vol. 8, Issue 1, 2013, pp. 24-56.

- [43] E. S. G. Maciel, and A. P., Pimenta, Thermochemical Non-Equilibrium Entry Flows in Mars in Two-Dimensions – Part II, *Submitted to Wseas Transactions on Mathematics* (under review).
- [44] E. S. G. Maciel, Relatório ao Conselho Nacional de Pesquisa e Desenvolvimento Tecnológico (CNPq) sobre as Atividades de Pesquisa Desenvolvidas no Primeiro Ano de Vigência da Bolsa de Estudos para Nível DCR-IF Referente ao Processo No. 304318/2003-5, *Report to the National Council of Scientific and Technological Development (CNPq)*, Recife, PE, Brazil, 37p, 2004. [available in the website www.edissonsavio.eng.br]
- [45] E. S. G. Maciel, Relatório ao Conselho Nacional de Pesquisa e Desenvolvimento Tecnológico (CNPq) sobre as Atividades de Pesquisa Desenvolvidas no Segundo Ano de Vigência da Bolsa de Estudos para Nível DCR-IF Referente ao Processo No. 304318/2003-5, *Report to the National Council of Scientific and Technological Development (CNPq)*, Recife, PE, Brazil, 54p, 2005. [available in the website www.edissonsavio.eng.br]
- [46] E. S. G. Maciel, and A. P., Pimenta, Thermochemical Non-Equilibrium Reentry Flows in Two-Dimensions: Eleven Species Model – Part I, *Submitted to the Wseas Transactions on Mathematics* (under review).